iScience

CellPress
OPEN ACCESS

Article

Simulating the Post-gastric Bypass Intestinal Microenvironment Uncovers a Barrier-Stabilizing Role for FXR

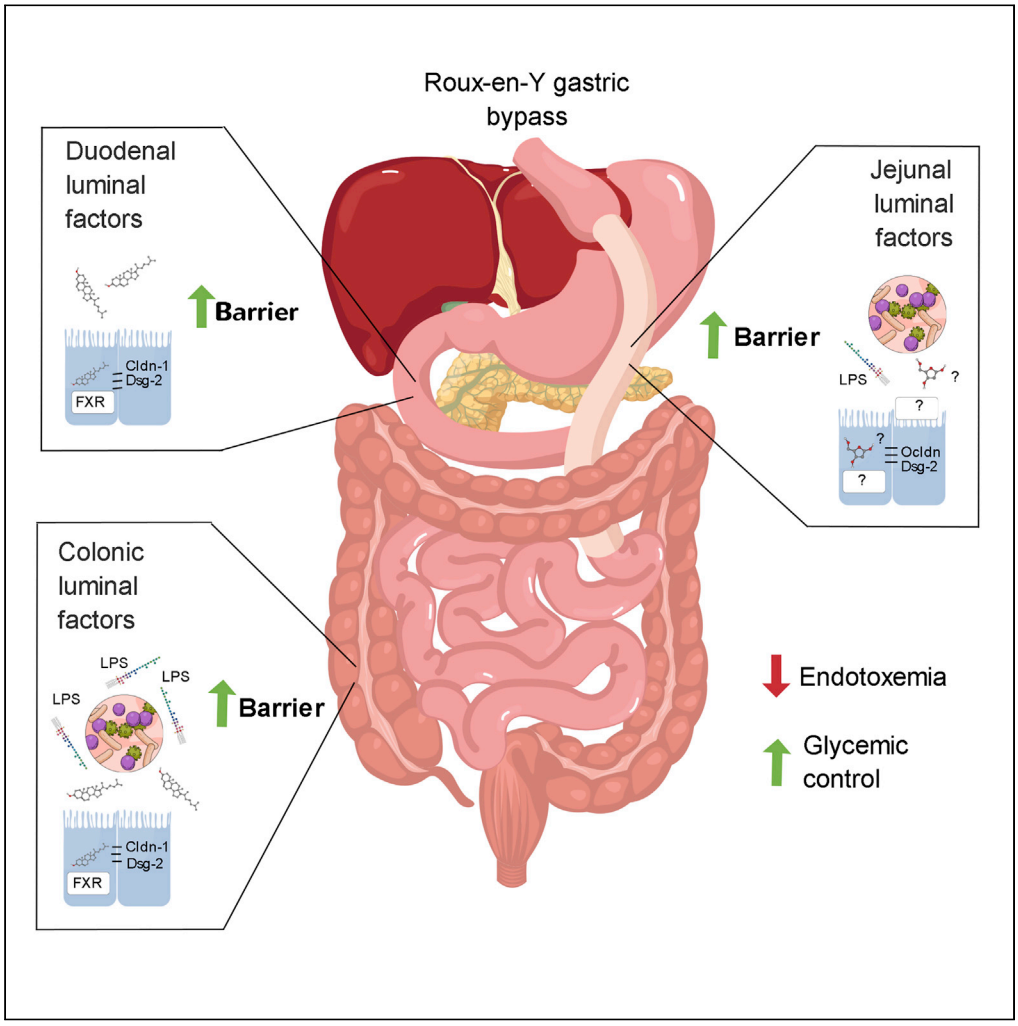

Mohammed K. Hankir, Theresa Langseder, Ezgi Eyluel Bankoglu, ..., Tulika Arora, Florian Seyfried, Nicolas Schlegel

hankir_m@ukw.de (M.K.H.)
schlegel_n@ukw.de (N.S.)

HIGHLIGHTS

RYGB intestinal contents improve glycemia and suppress endotoxemia in GF mice

RYGB intestinal contents stabilize barrier function and structure in Caco-2 cells

This is partly FXR-dependent for bile-exposed intestinal contents only

Plasma bile acids and FGF19 negatively correlate with endotoxemia in RYGB patients

Hankir et al., iScience *23*, 101777
December 18, 2020
https://doi.org/10.1016/j.isci.2020.101777

iScience

CellPress
OPEN ACCESS

Article

Simulating the Post-gastric Bypass Intestinal Microenvironment Uncovers a Barrier-Stabilizing Role for FXR

Mohammed K. Hankir,[1,6,*] Theresa Langseder,[1] Ezgi Eyluel Bankoglu,[2] Yalda Ghoreishi,[1] Ulrich Dischinger,[3] Max Kurlbaum,[3] Matthias Kroiss,[3] Christoph Otto,[1] Carel W. le Roux,[4] Tulika Arora,[5] Florian Seyfried,[1] and Nicolas Schlegel[1,*]

SUMMARY

Regional changes to the intestinal microenvironment brought about by Roux-en-Y gastric bypass (RYGB) surgery may contribute to some of its potent systemic metabolic benefits through favorably regulating various local cellular processes. Here, we show that the intestinal contents of RYGB-operated compared with sham-operated rats region-dependently confer superior glycemic control to recipient germ-free mice in association with suppression of endotoxemia. Correspondingly, they had direct barrier-stabilizing effects on an intestinal epithelial cell line which, bile-exposed intestinal contents, were partly farnesoid X receptor (FXR)-dependent. Further, circulating fibroblast growth factor 19 levels, a readout of intestinal FXR activation, negatively correlated with endotoxemia severity in longitudinal cohort of RYGB patients. These findings suggest that various host- and/or microbiota-derived luminal factors region-specifically and synergistically stabilize the intestinal epithelial barrier following RYGB through FXR signaling, which could potentially be leveraged to better treat endotoxemia-induced insulin resistance in obesity in a non-invasive and more targeted manner.

INTRODUCTION

No currently available, non-surgical treatment intervention for morbid obesity approaches the clinical efficacy of metabolic surgeries such as Roux-en-Y gastric bypass (RYGB) (Ruban et al., 2019). By creating a small gastric pouch and adjoining it to the transected mid-jejunum, in combination with adjoining the freed upper to the lower jejunum, RYGB typically achieves 30–40% weight loss, which is sustained in the long-term (Adams et al., 2016; Sjostrom et al., 2004, 2007), and, in most cases, rapid remission of type 2 diabetes (Mingrone et al., 2012, 2015; Panunzi et al., 2016). Numerous surgery-specific mechanisms have been proposed for this remarkable restoration of glycemic control post-operatively, including loss of upper jejunal glucose absorption from ingested food by the apical sodium-glucose co-transporters 1/3 (Baud et al., 2016; Pal et al., 2019; Stearns et al., 2009), increased lower jejunal glucose extraction from the circulation by the basolateral glucose transporter 1 (Cavin et al., 2016; Makinen et al., 2015; Pal et al., 2019; Saeidi et al., 2013), as well as gut hormone-mediated improvements in pancreatic islet cell function (Guida et al., 2019; Jorgensen et al., 2013; Ramracheya et al., 2016; Salehi et al., 2014). In addition, circulating bile acid levels steeply rise (Ahlin et al., 2019; Bhutta et al., 2015; Chen et al., 2019; Ferrannini et al., 2015; Gerhard et al., 2013; Kohli et al., 2013; Pournaras et al., 2012; Spinelli et al., 2016; Yan et al., 2019; Zhai et al., 2018) and circulating branched chain amino acid levels decline (Laferrere et al., 2011; Lips et al., 2014; Yoshino et al., 2020) in association with favorable shifts in the intestinal microbiota (Arora et al., 2017; Liou et al., 2013; Tremaroli et al., 2015). Despite significant progress in the field, further understanding precisely how these changes add or contribute to the restored hepatic and peripheral insulin sensitivities that appear to develop sequentially following RYGB (Albers et al., 2015; Bikman et al., 2008; Bojsen-Moller et al., 2014; Campos et al., 2010; Chambers et al., 2011; Gancheva et al., 2019; He et al., 2014; Lima et al., 2010; Martinussen et al., 2015; Meirelles et al., 2009; Steven et al., 2016; Yoshino et al., 2020) will invariably inform the design of more effective pharmacotherapies against insulin resistance and type 2 diabetes.

The intestinal epithelial barrier (IEB) comprises a single continuous layer of cells lining the gastrointestinal tract and serves as the main line of defense against ingested toxins and potentially pathogenic microbes

[1]Department of General, Visceral, Transplant, Vascular and Pediatric Surgery, University Hospital Wuerzburg, Center of Operative Medicine, Oberduerrbacherstrasse 6, Wuerzburg, Bavaria 97080, Germany

[2]Institute of Pharmacology and Toxicology, University of Wuerzburg, Wuerzburg, Bavaria 97080, Germany

[3]Department of Endocrinology and Diabetology, University Hospital Wuerzburg, Wuerzburg, Bavaria 97080, Germany

[4]Diabetes Complications Research Centre, University College Dublin, Dublin 4, Ireland

[5]Novo Nordisk Foundation Centre for Basic Metabolic Research, University of Copenhagen, Copenhagen, 2200, Denmark

[6]Lead Contact

*Correspondence: hankir_m@ukw.de (M.K.H.), schlegel_n@ukw.de (N.S.)

https://doi.org/10.1016/j.isci.2020.101777

residing in the gastrointestinal wall and lumen (Vancamelbeke and Vermeire, 2017). Tight junctions, adherens junctions, and desmosomes are multi-protein complexes located to the cell membrane of enterocytes that together form a homophilic, tripartite seal from the apical to the basolateral sides, respectively (Garcia et al., 2018; Heinemann and Schuetz, 2019; Schlegel et al., 2020). Since the original findings in mice (Cani et al., 2007, 2008), evidence has mounted that obesity is associated with IEB breakdown primarily due to unfavorable shifts in the intestinal microbiota caused by frequent overconsumption of a high-fat diet (Chakaroun et al., 2020). Consequently, bacteria and their components such as lipopolysaccharide (LPS) leak into the circulation and accumulate in metabolic tissues, where they induce a chronic, low-grade state of inflammation leading to local and systemic insulin resistance (Chakaroun et al., 2020). Stabilizing the IEB in obesity either by small molecule drugs (Lin et al., 2019; Luck et al., 2015; Natividad et al., 2018) or by microbiota transplant (Depommier et al., 2019; Natividad et al., 2018; Wang et al., 2019b) thus shows promise in attenuating endotoxemia-induced insulin resistance.

Whether RYGB stabilizes the IEB to impact on glycemic control has been addressed in several clinical and pre-clinical studies. Early findings from pre-diabetic/diabetic patients revealed that RYGB reduces plasma LPS/LPS binding protein (LBP) levels to those of healthy lean individuals associated with a reduction in fasting plasma glucose, glycated hemoglobin (HbA1c), and insulin levels (Monte et al., 2012; Troseid et al., 2013; Yang et al., 2014). Similarly, RYGB has been shown to reduce intestinal permeability in diet-induced obese mice (Steensels et al., 2017) and rats (Wang et al., 2019a), as well as to normalize plasma LPS levels and glycemic status in streptozotocin-induced diabetic (Wu et al., 2019) and genetically obese and insulin-resistant Zucker diabetic fatty (ZDF) (Guo et al., 2019) rats. Collectively, these clinical and pre-clinical findings strongly suggest that at the later stages post-operatively (Guo et al., 2019; Monte et al., 2012; Steensels et al., 2017; Troseid et al., 2013; Wang et al., 2019a; Wu et al., 2019; Yang et al., 2014), RYGB improves glycemic control by stabilizing the IEB and attenuating endotoxemia-induced insulin resistance; however, the underlying molecular and cellular mechanisms remain poorly understood. We previously found that the improved oral glucose tolerance in genetically obese and glucose-intolerant Zucker fatty (ZF) rats following RYGB compared with sham surgery can be transmitted through their cecal, but not their ileal, contents to recipient germ-free mice (Arora et al., 2017). We therefore hypothesized that soluble factors within the intestinal contents of RYGB-operated rats region-specifically regulate IEB stability to exert distinct effects on endotoxemia and glycemic control.

RESULTS

RYGB Improves Metabolic Parameters and Attenuates Endotoxemia in Diet-Induced Obese Rats

We first metabolically phenotyped a cohort of adult male Wistar rats made obese on a high-fat diet and then subjected to either RYGB or sham surgeries (Figure S1). Post-operatively, animals were given simultaneous free access to both high-fat and low-fat diets to model the real-world situation in humans and assess changes in food choice (Dischinger et al., 2019; Hankir et al., 2017) (Figure 1A). In line with previous findings (Dischinger et al., 2019; Hankir et al., 2017), RYGB-operated compared with sham-operated rats consumed less food over the 3-week recording period (1318 $\pm$ 90.6 kcal vs. 1889 $\pm$ 52.2 kcal, respectively, $P < 0.0001$; Figure 1B). They also progressively obtained more of their daily calories from the low-fat diet rather than from the high-fat diet, unlike sham-operated rats (Figure 1C). Accordingly, RYGB-operated rats weighed considerably less than their sham-operated counterparts at the time of sacrifice 6 weeks after surgeries (451.9 $\pm$ 12.5 g vs. 592.6 $\pm$ 13.9 g, respectively, $P < 0.0001$; Figure 1D), which equated to a 23.7 $\pm$ 2.1% difference (Figure 1E), and had lower fasting plasma insulin (Figure 1F) and LPS (Figure 1G) levels. Together, these findings provide confidence that our rat model closely matches the clinical features of RYGB by improving eating behavior and reducing body weight in association with attenuated insulinemia and endotoxemia.

The Jejunal and Colonic Contents of RYGB-Operated Rats Confer Superior Glycemic Control to Recipient Germ-free Mice in Association with Suppression of Endotoxemia

Next, to test our hypothesis that the intestinal contents region-specifically regulate glycemic control and endotoxemia following RYGB, we transferred the jejunal and colonic contents of RYGB-operated and sham-operated rats to germ-free mice and performed oral glucose tolerance tests (OGTTs) 2 weeks later in conjunction with serum LBP measurements, a reliable indicator of endotoxemia (Guerville et al., 2017; Moreno-Navarrete et al., 2012) (Figure 2A). We have previously shown that such transfer leads to colonization of the gastrointestinal tract of recipient germ-free mice with the microbiota present in the intestinal

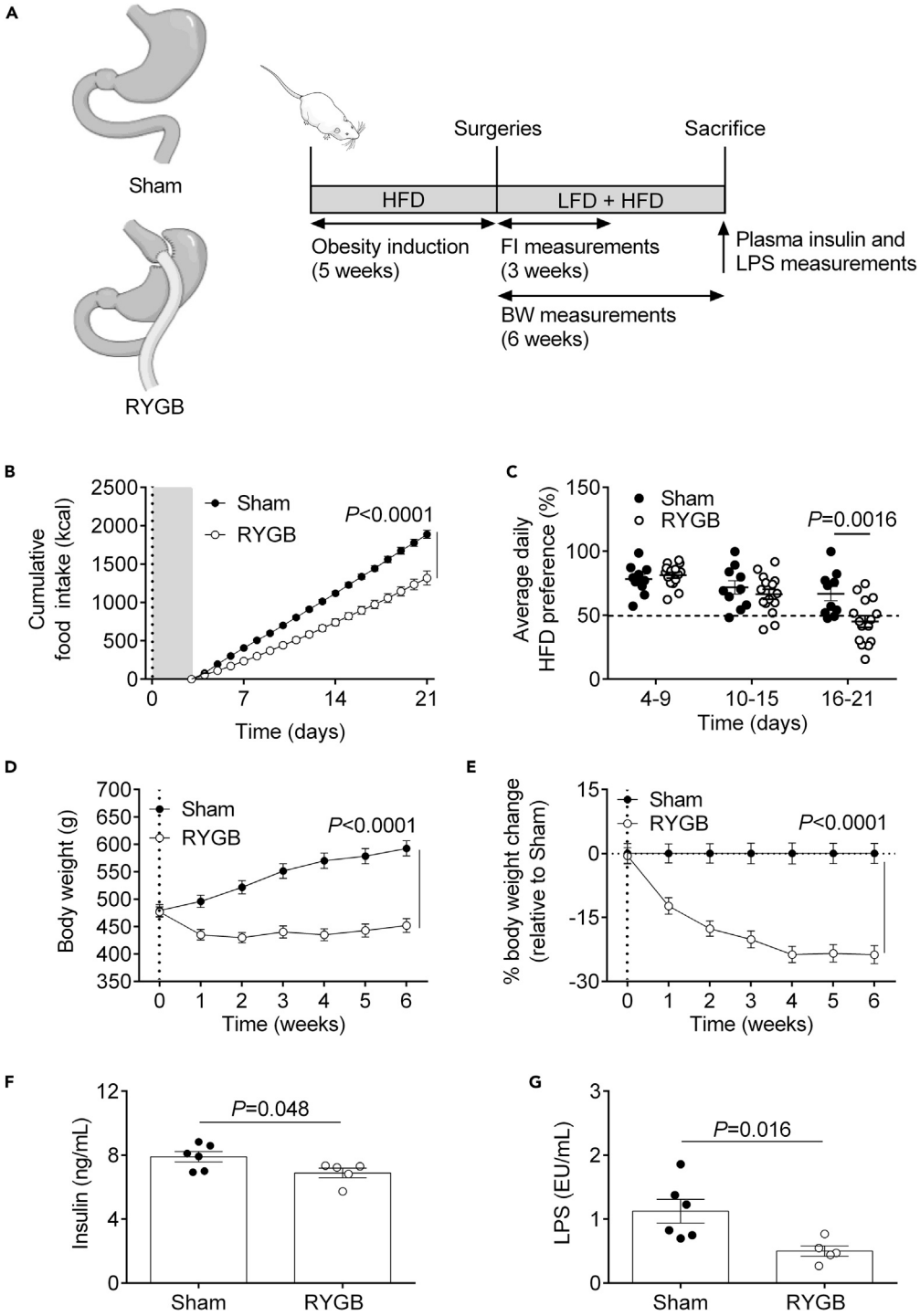

Figure 1. RYGB Improves Metabolic Parameters and Attenuates Endotoxemia in Diet-Induced Obese Wistar Rats

(A) Schematic diagram illustrating experiments performed on sham-operated (Sham) and RYGB-operated (RYGB) rats.

(B and C) Cumulative total food intake (B) and average daily high-fat diet (HFD) preference (C) of Sham (n = 10) and RYGB (n = 15) rats over the 21-day recording period after surgeries. Dashed vertical line and gray panel in (B) indicate time of surgeries and 3-day recovery period when animals were placed on a liquid diet, respectively. Dashed horizontal line in (C) indicates equal preference for HFD and low-fat diet (LFD).

(D and E) Body weight of Sham (n = 10) and RYGB (n = 15) rats (D) and percentage (%) body weight change relative to Sham rats (E) over the 6-week recording period after surgeries. Dashed vertical lines in (D and E) indicate time of surgeries.

Figure 1. *Continued*
(F and G) Fasting plasma insulin (F) and lipopolysaccharide (LPS) (G) levels of a subset of Sham ($n = 6$) and RYGB ($n = 5$) rats at the time of sacrifice 6 weeks after surgeries.
Data in (B-G) are presented as mean ± SEM. Statistical significance was determined by two-way ANOVA (main effect of treatment) in (B-E) with Sidak's post-hoc test in (C) and two-tailed, unpaired *t* test in (F and G).
See also Figure S1.

contents of rat donors (Arora et al., 2017). We found that the jejunal contents of RYGB-operated compared with sham-operated rats conferred marginally better blood glucose clearing capability to recipient germ-free mice (Figure 2B). This was largely driven by the lower peak blood glucose levels at 15 min after the oral glucose challenge and the greater drop in blood glucose levels 15 min later (Figure 2B). On the other hand, the colonic contents of RYGB-operated compared with sham-operated rats had a more pronounced beneficial effect on glycemic control in recipient germ-free mice as their blood glucose levels were lower at all time-points after the oral glucose challenge (Figure 2D). Notably, germ-free mice that had received the contents from both intestinal regions of RYGB-operated compared with sham-operated rats had lower serum LBP levels (Figures 2C and 2D). When merging the data from both surgical treatment groups (Li et al., 2019), regression analysis revealed a positive correlation between serum LBP levels in recipient germ-free mice and the area under the curve (AUC) from their OGTTs (Figure 2F). In contrast, the duodenal contents of RYGB-operated compared with sham-operated, ZF rats had no effect on oral glucose tolerance in recipient germ-free mice (Figure S2). These findings provide evidence that the altered jejunal and colonic, but not duodenal, contents following RYGB improve glycemic control in recipient germ-free mice in association with suppression of endotoxemia.

The Intestinal Contents of RYGB-Operated Rats Directly Stabilize Barrier Function and Structure in Caco-2 Cells

Having established that the intestinal contents of RYGB-operated compared with sham-operated rats favor the suppression of endotoxemia in recipient germ-free mice, we then proceeded to ask in more detail if they contain soluble factors that directly regulate IEB stability. To do so, we partially simulated the regional intestinal microenvironments of RYGB-operated and sham-operated rats by applying their duodenal, jejunal, and colonic contents onto the apical side of confluent Caco-2 cell monolayers, a human colonic cancer cell line differentiated into polarized enterocytes routinely used to test factors that regulate IEB function and structure (Lea, 2015) (Figure 3A). We note that because cell culture media was supplemented with antibiotics for these experiments (see Transparent Methods), a static simulation was achieved; that is, only microbiota-derived soluble factors *already* present in the intestinal contents upon collection could potentially exert effects in this setting.

For our functional experiments, we took two complementary approaches. We first performed measurements of 4 kDa fluorescein isothiocyanate (FITC)-dextran paracellular flux from the apical to the basolateral sides of Caco-2 cells in trans-well assays, followed by transepithelial electrical resistance (TER) measurements between Caco-2 cells in low-frequency electrical impedance assays. This revealed that the duodenal, jejunal, and colonic contents of RYGB-operated compared with sham-operated rats markedly decreased 4 kDa FITC-dextran passage across Caco-2 cells (reflected by decreased epithelial permeability coefficients - P_E) (Figures 3B–3D). Accordingly, they all markedly increased TER values (Figures 3E–3G).

For our structural analyses, we also took two complementary approaches. We first performed immunoblot analysis to determine overall barrier protein expression in Caco-2 cells treated with the duodenal, jejunal, and colonic contents of RYGB-operated and sham-operated rats, followed by high-magnification immunofluorescent analysis to determine their cellular distribution in response to the same treatments (Tables S1 and S2 for antibody details). This revealed that the duodenal and colonic contents of RYGB-operated compared with sham-operated rats increased expression of the barrier-stabilizing tight junction protein claudin-1 (Garcia-Hernandez et al., 2017) and the barrier-stabilizing desmosomal protein desmoglein-2 (Schlegel et al., 2020) (Figures 3H and 3J). On the other hand, the jejunal contents of RYGB-operated compared with sham-operated rats increased expression of the barrier-stabilizing tight junction protein occludin (Garcia-Hernandez et al., 2017), as well as desmoglein-2 (Figure 3I). High-magnification immunofluorescent analysis was largely consistent with the immunoblot findings (Figures 3K-M), with the addition that the jejunal contents of RYGB-operated compared with sham-operated rats increased claudin-1 protein at the cell border of Caco-2 cells (Figure 3L).

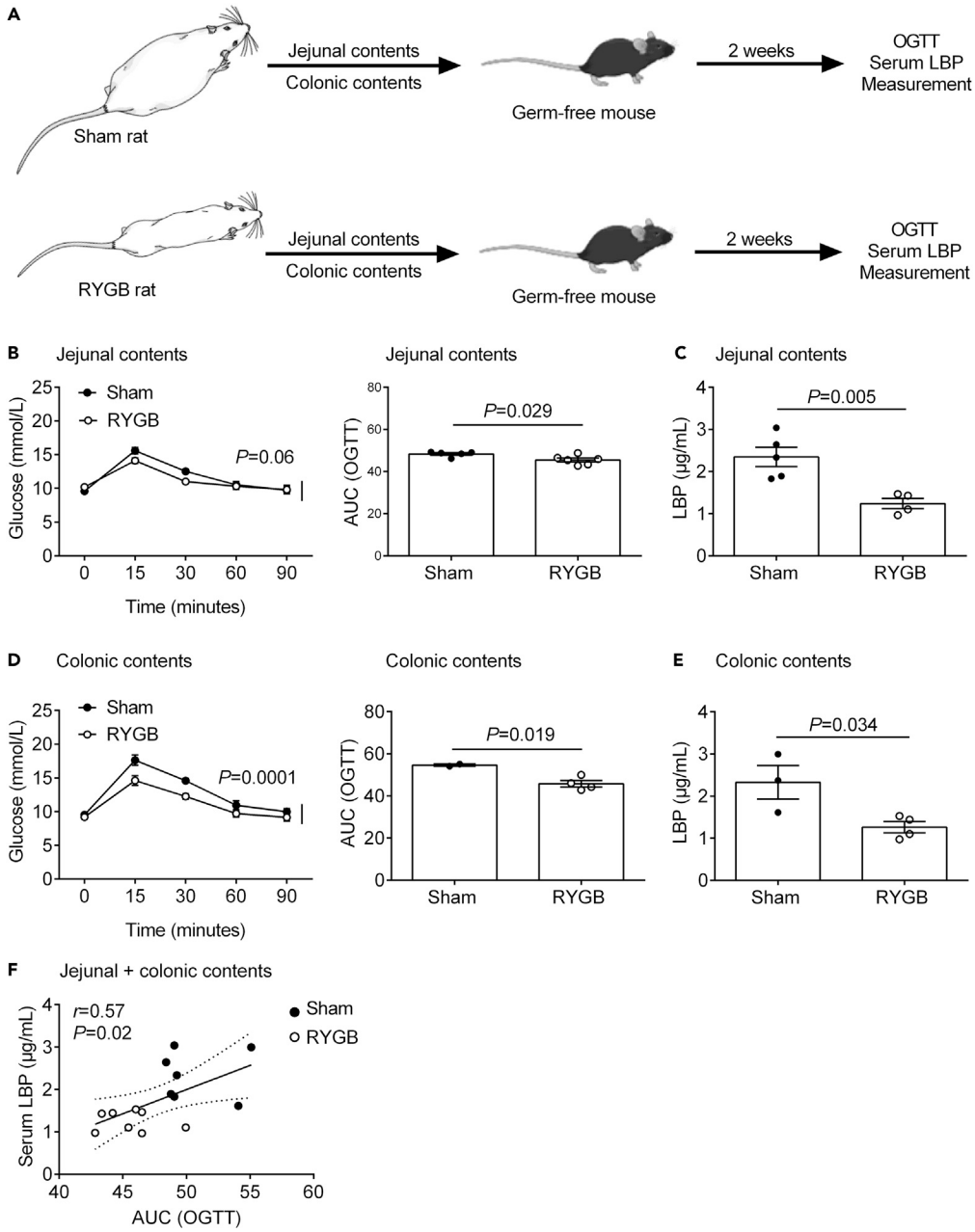

Figure 2. The Jejunal and Colonic Contents of RYGB-Operated Rats Confer Superior Glycemic Control to Recipient Germ-Free Mice in Association with Suppression of Endotoxemia

(A) Schematic diagram illustrating the jejunal and colonic contents transfer experiments and oral glucose tolerance tests (OGTTs) performed on recipient germ-free mice.

(B and C) Tail vein blood glucose concentrations following an oral glucose challenge with the associated area under the curve (AUC) (B) and serum LPS binding protein (LBP) concentrations (C) of germ-free mice that had received the pooled jejunal contents of Sham or RYGB rats. n = 4–6 mice/group.

(D and E) Tail vein blood glucose concentrations following an oral glucose challenge with the associated AUC (D) and serum LBP concentrations (E) of germ-free mice that had received the pooled colonic contents of Sham or RYGB rats. n = 3–4 mice/group.

(F) Pearson correlation between AUC from OGTTs and serum LBP of germ-free mice from (B, C, E, and F). Solid regression lines indicate least squares fit of data and dashed lines indicate 95% confidence intervals.

Data in (B-E) are presented as mean ± SEM. Statistical significance was determined by two-way ANOVA (main effect of treatment) in (B and D) and two-tailed, unpaired t test in (B–E and F).

See also Figure S2.

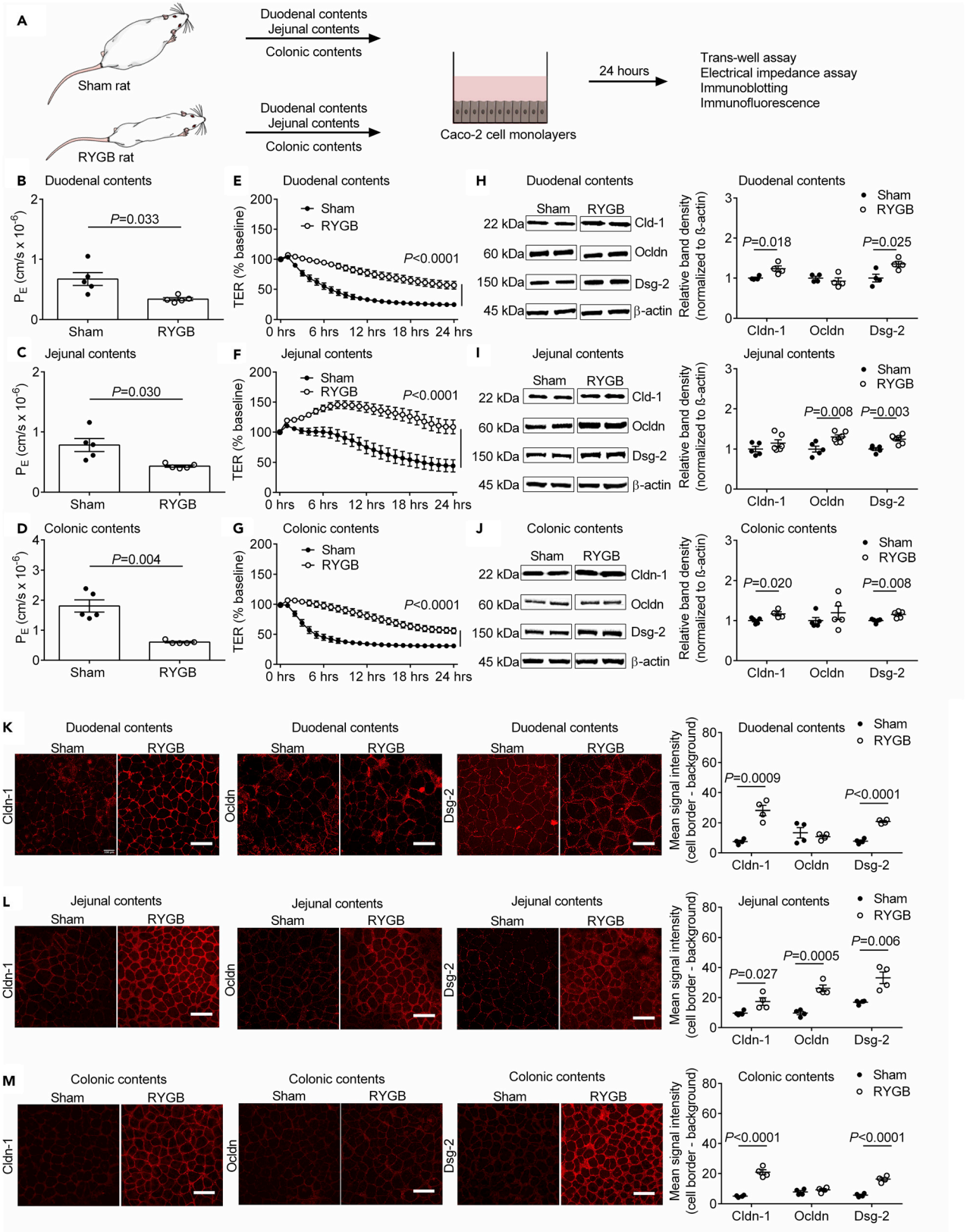
A
Sham rat
RYGB rat
Duodenal contents
Jejunal contents
Colonic contents
Caco-2 cell monolayers
24 hours
Trans-well assay
Electrical impedance assay
Immunoblotting
Immunofluorescence
B Duodenal contents
P=0.033
Sham
RYGB
C Jejunal contents
P=0.030
D Colonic contents
P=0.004
E Duodenal contents
P<0.0001
TER (% baseline)
0 hrs 6 hrs 12 hrs 18 hrs 24 hrs
F Jejunal contents
G Colonic contents
H Duodenal contents
22 kDa Cld-1
60 kDa Ocldn
150 kDa Dsg-2
45 kDa β-actin
I Jejunal contents
J Colonic contents
Relative band density (normalized to β-actin)
P=0.018
P=0.025
P=0.008
P=0.003
P=0.020
P=0.008
Cldn-1
Ocldn
Dsg-2
K Duodenal contents
L Jejunal contents
M Colonic contents
Mean signal intensity (cell border - background)
P=0.0009
P<0.0001
P=0.027
P=0.0005
P=0.006
P<0.0001
P<0.0001

Figure 3. The Intestinal Contents of RYGB-Operated Rats Directly Stabilize Barrier Function and Structure in Caco-2 Cells

(A) Schematic diagram illustrating intestinal microenvironment simulation experiments performed on Caco-2 cells.

(B–D) Permeability coefficients (P_E) obtained from trans-well assays performed on confluent Caco-2 cell monolayers treated for 24 hr with the pooled duodenal (B), jejunal (C), and colonic (D) contents of Sham and RYGB rats. *n* = 5 cultures/group from 1 independent experiment.

(E–G) Trans-epithelial electrical resistance (TER) values obtained from low-frequency electrical impedance assays performed on confluent Caco-2 cell monolayers treated for 24 hr with the pooled duodenal (E), jejunal (F), and colonic (G) contents of Sham and RYGB rats. *n* = 16 cultures/group from 2 independent experiments.

(H–J) Immunoblot analysis of claudin-1 (Cldn-1), occludin (Ocldn), and desmoglein-2 (Dsg-2) protein expression in confluent Caco-2 cell monolayers treated for 24 hr with the pooled duodenal (H), jejunal (I), and colonic (J) contents of Sham and RYGB rats. n = 5–6 cultures/group from 1 independent experiment.

(K–M) Immunofluorescent analysis of Cldn-1, Ocldn, and Dsg-2 protein expression and distribution in confluent Caco-2 cell monolayers treated for 24 hr with the pooled duodenal (K), jejunal (L), and colonic (M) contents of Sham and RYGB rats. Scale bar: 25μm.

Data in (B-K) are presented as mean ± SEM. Statistical significance was determined by two-tailed, unpaired *t* test with Welch's correction in (B-D), two-way ANOVA (main effect of treatment) in (E-G), and two-tailed, unpaired *t* test in (H–M).

See also Figure S3.

In order to assess potential differences in the transcription of barrier proteins in Caco-2 cells in response to the duodenal, jejunal, and colonic contents of RYGB-operated compared with sham-operated rats, we performed real-time quantitative polymerase chain reaction (RT-qPCR) analysis (See Table S3 for primer sequences). This revealed no significant effect on *CLDN1*, *OCLDN*, and *DSG2* mRNA expressions (Figure S3), suggesting that post-transcriptional processes mainly drive the observed regulation of barrier proteins under our *in vitro* experimental conditions. Such a dissociation between mRNA and protein expression levels of various barrier proteins has also been shown for intestinal enteroids derived from patients with inflammatory bowel disease compared with healthy patients (Meir et al., 2020). Together, these findings reveal that the duodenal, jejunal, and colonic contents following RYGB contain soluble factors that directly stabilize IEB function and structure. In conjunction with the germ-free mice findings, they further suggest dissociation between regulation of IEB stability and endotoxemia by the intestinal contents of RYGB-operated compared with sham-operated rats.

The Duodenal and Colonic, but not the Jejunal, Contents of RYGB-Operated Rats Stabilize Barrier Function Partly through FXR in Caco-2 Cells

Genetic inactivation of the bile acid receptors Takeda G-protein–coupled receptor 5 (TGR5) and farnesoid X receptor (FXR) leads to IEB breakdown in mice (Cipriani et al., 2011; Inagaki et al., 2005b), whereas TGR5 and FXR agonists, including the intestinally restricted FXR agonist fexaramine, have barrier-stabilizing properties in multiple settings (Cipriani et al., 2011; Fang et al., 2015; Hartmann et al., 2018; Sorribas et al., 2019; Verbeke et al., 2015). Furthermore, while TGR5 and/or FXR are required for the full beneficial effects on glycemic control of various metabolic surgeries including RYGB (Li et al., 2020) and vertical sleeve gastrectomy (VSG) (Ding et al., 2016; McGavigan et al., 2017; Ryan et al., 2014) in diet-induced obese mice, it is unknown whether this is through regulating IEB stability. We therefore tested the effects of the duodenal, jejunal, and colonic contents of RYGB-operated compared with sham-operated rats in electrical impedance assays performed on Caco-2 cell monolayers in the presence of selective TGR5/FXR antagonists/agonists compared with vehicle control (Figure 4).

In order to gain insight into whether intestinal bile acid receptors region-specifically contribute to stabilization of the IEB following RYGB, the duodenal, jejunal, and colonic contents of RYGB-operated rats were supplemented with the TGR5 antagonist triamterene (10μM) (Cheng et al., 2019; Li et al., 2017; Lo et al., 2017; Wang et al., 2017a, 2017b) or the selective FXR antagonist DY-268 (10μM) (Yu et al., 2014). This revealed that only the latter treatment partially negated the effects on TER values of the duodenal and the colonic (Figures 4B and 4F), but not the jejunal (Figure 4D), contents of RYGB-operated rats. These findings suggest that duodenal and colonic luminal factors following RYGB improve IEB function partly through FXR, whereas jejunal luminal factors do so independently of FXR.

In order to gain insight into whether intestinally restricted bile acid receptor agonists could region-specifically stabilize the IEB in obesity, the duodenal, jejunal, and colonic contents of sham-operated rats were supplemented with the selective TGR5 agonist 3-(2-chlorophenyl)-N-(4-chlorophenyl)-N, 5-dimethyl-4-isoxazolecarboxamide (10μM) (Evans et al., 2009) or the selective FXR agonist WAY-362450 (10μM) (Flatt et al., 2009). This revealed that only the latter treatment modestly increased TER values in response to the duodenal and the colonic (Figures 4B and 4F), but not the jejunal (Figure 4D), contents of sham-operated rats. These findings suggest that soluble factors specifically in the duodenal and colonic contents following RYGB act in synergy with FXR agonism to stabilize IEB function.

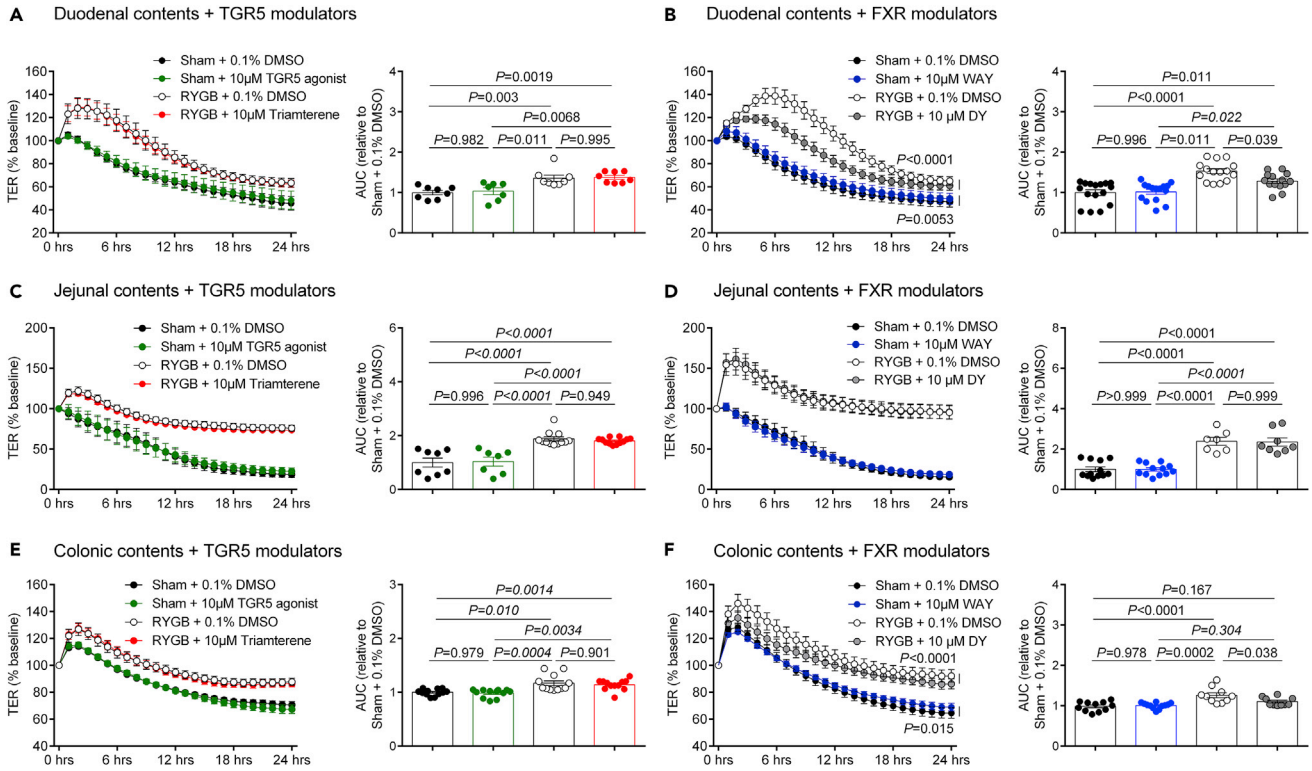

Figure 4. The Duodenal and Colonic, but not the Jejunal, Contents of RYGB-Operated Rats Stabilize Barrier Function Partly through FXR in Caco-2 Cells

(A–F) TER measurements and associated AUCs obtained from low-frequency electrical impedance assays performed on confluent Caco-2 cell monolayers treated for 24 hr with the pooled duodenal (A and B), jejunal (C and D), and colonic (D and E) contents of Sham and RYGB rats in the presence of 10μM of the TGR5 agonist 3-(2-chlorophenyl)-N-(4-chlorophenyl)-N,5-dimethyl-4-isoxazolecarboxamide (TGR5 agonist), 10μM of the TGR5 antagonist triamterene, 10uM of the FXR agonist WAY-362450 (WAY), 10 μM of the FXR antagonist DY-268 (DY), or vehicle control (0.1% DMSO). *n* = 7–16 cultures/group from 1 to 2 independent experiments.

Data are presented as mean ± SEM. Statistical significance was determined by two-way ANOVA (main effect of treatment) in (B and F) and one-way ANOVA with Tukey's post-hoc test in (A-F).

Plasma Cholic acid, Chenodeoxycholic acid, and FGF19 Levels Negatively Correlate with Endotoxemia Severity in Pre-diabetic/Diabetic RYGB Patients

In order to translate our animal and cell-based findings, we revisited phenotypic data and re-analyzed fasting plasma samples previously obtained from a mixed longitudinal cohort of 38 pre-diabetic/diabetic patients at baseline and 12 months after RYGB (Bankoglu et al., 2018). As expected, RYGB markedly reduced body weight, BMI, fasting plasma leptin, and LPS levels (Table 1). This was associated with a reduction in various circulating pro-inflammatory cytokines/markers such as tumor necrosis factor-alpha (TNF-α), interleukin-6 (Il-6), and C-reactive protein, which is in-line with previous studies (Illan-Gomez et al., 2012; Viana et al., 2013), as well as an improvement in several markers of glycemic status including fasting plasma HbA1c, glucose, and insulin levels, which drove homeostatic model of insulin resistance (HOMA-IR) indices down (Table 1).

We next measured fasting plasma bile acid levels by electrospray ionization liquid chromatography–mass spectrometry (ESI-LC-MS/MS). In-line with previous studies (Ahlin et al., 2019; Chen et al., 2019; Gerhard et al., 2013; Kohli et al., 2013; Pournaras et al., 2012; Spinelli et al., 2016), this revealed an approximately order of magnitude increase for the unconjugated primary bile acids cholic acid (CA) and chenodeoxycholic acid (CDCA), as well as comparatively smaller (approximately 50%) increases in their glycine-conjugated derivatives glycocholic acid (GCA) and glycochenodeoxycholic acid (GCDCA) 12 months after RYGB compared with baseline (Table 2). Similarly, for secondary bile acids, there was a 4-fold increase in deoxycholic acid (DCA) and a 2-fold increase in ursodeoxycholic acid (UDCA) along with a corresponding increase in glycodeoxycholic acid (GDCA), whereas glycoursodeoxycholic acid (GUDCA) did not change

Metabolic Parameter	Baseline	12 months Post-RYGB	p Value
Body weight (kg)	146.5 ± 3.1 (*n* = 38)	104.3 ± 3.7 (*n* = 34)	**≤0.0001**
Body mass index (kg/m^2)	51.2 ± 1.0 (*n* = 38)	36.4 ± 1.1 (*n* = 34)	**≤0.0001**
Plasma leptin (ng/mL)	29.58 ± 2.17 (*n* = 37)	9.47 ± 1.51 (*n* = 23)	**≤0.0001**
Plasma LPS (EU/mL)	0.42 ± 0.02 (*n* = 34)	0.32 ± 0.04 (*n* = 26)	**≤0.0001**
Plasma Tnf-α (pg/mL)	4.10 ± 0.40 (*n* = 37)	3.11 ± 0.33 (*n* = 23)	**0.0035**
Plasma Il-6 (pg/mL)	10.42 ± 2.42 (*n* = 37)	5.94 ± 1.84 (*n* = 23)	**0.0081**
Plasma CrP (μg/mL)	93.76 ± 9.84 (*n* = 37)	28.89 ± 6.06 (*n* = 35)	**≤0.0001**
Plasma HbA1c (%)	5.77 ± 0.11 (*n* = 31)	5.26 ± 0.07 (*n* = 33)	**≤0.0001**
Plasma glucose (mg/mL)	9.4 ± 0.19 (*n* = 37)	8.6 ± 0.15 (*n* = 33)	**0.0004**
Plasma insulin (ng/mL)	0.64 ± 0.09 (*n* = 37)	0.23 ± 0.03 (*n* = 23)	**≤0.0001**
HOMA-IR	3.10 ± 0.38 (*n* = 34)	1.15 ± 0.18 (*n* = 20)	**≤0.0001**

Table 1. Fasting Metabolic Parameters of Pre-diabetic/diabetic RYGB Patients at Baseline and 12 Months after Surgery

Data are presented as mean ± SEM. p Values in bold are statistically significant as determined by two-tailed, paired *t* test or Wilcoxan matched-pairs signed rank test.

(Table 2). Interestingly, while fasting plasma lithocholic acid (LCA) levels also did not change 12 months after RYGB compared with baseline, there was a significant increase in glycolithocholic acid (GLCA) (Table 2).

Because CA, CDCA, GCA, GCDCA, DCA, and GLCA are all FXR agonists (Parks et al., 1999; Wang et al., 1999), and fibroblast growth factor 15/19 (FGF15/19) is released from enterocytes in response to activation of FXR (Inagaki et al., 2005a), we measured fasting plasma FGF19 levels in patients at baseline and 12 months after RYGB. In-line with previous studies (Chen et al., 2019; DePaoli et al., 2019; Gerhard

Plasma BIle Acid or Related Factor	Baseline	12 months Post-RYGB	p Value
CA (μmol/L)	0.146 ± 0.05 (*n* = 37)	1.65 ± 0.57 (*n* = 27)	**0.0047**
CDCA (μmol/L)	0.22 ± 0.06 (*n* = 37)	1.60 ± 0.38 (*n* = 27)	**0.0061**
GCA (μmol/L)	0.28 ± 0.06 (*n* = 37)	0.37 ± 0.07 (*n* = 27)	0.071
GCDCA (μmol/L)	0.81 ± 0.13 (*n* = 37)	1.27 ± 0.19 (*n* = 27)	**0.031**
Total primary bile acids (μmol/L)	1.47 ± 0.26 (*n* = 37)	4.90 ± 0.93 (*n* = 27)	**0.0024**
DCA (μmol/L)	0.23 ± 0.03 (*n* = 37)	0.96 ± 0.20 (*n* = 27)	**0.0051**
LCA (μmol/L)	0.023 ± 0.002 (*n* = 37)	0.021 ± 0.002 (*n* = 27)	0.64
UDCA (μmol/L)	0.06 ± 0.01 (*n* = 37)	0.12 ± 0.03 (*n* = 27)	0.17
GDCA (μmol/L)	0.32 ± 0.08 (*n* = 37)	0.52 ± 0.09 (*n* = 27)	0.26
GLCA (μmol/L)	0.009 ± 0.001 (*n* = 37)	0.013 ± 0.002 (*n* = 27)	**0.037**
GUDCA (μmol/L)	0.09 ± 0.01 (*n* = 37)	0.09 ± 0.02 (*n* = 27)	0.58
Total secondary bile acids (μmol/L)	0.70 ± 0.09 (*n* = 37)	1.74 ± 0.26 (*n* = 27)	**0.0079**
FGF 19 (pg/mL)	22.76 ± 2.95 (*n* = 33)	63.72 ± 11.79 (*n* = 20)	**0.0006**

Table 2. Fasting Plasma Bile Acid and FGF19 Concentrations of Pre-diabetic/Diabetic RYGB Patients at Baseline and 12 Months after Surgery

Data are presented as mean ± SEM. p values in bold are statistically significant as determined by Wilcoxan matched-pairs signed rank test.

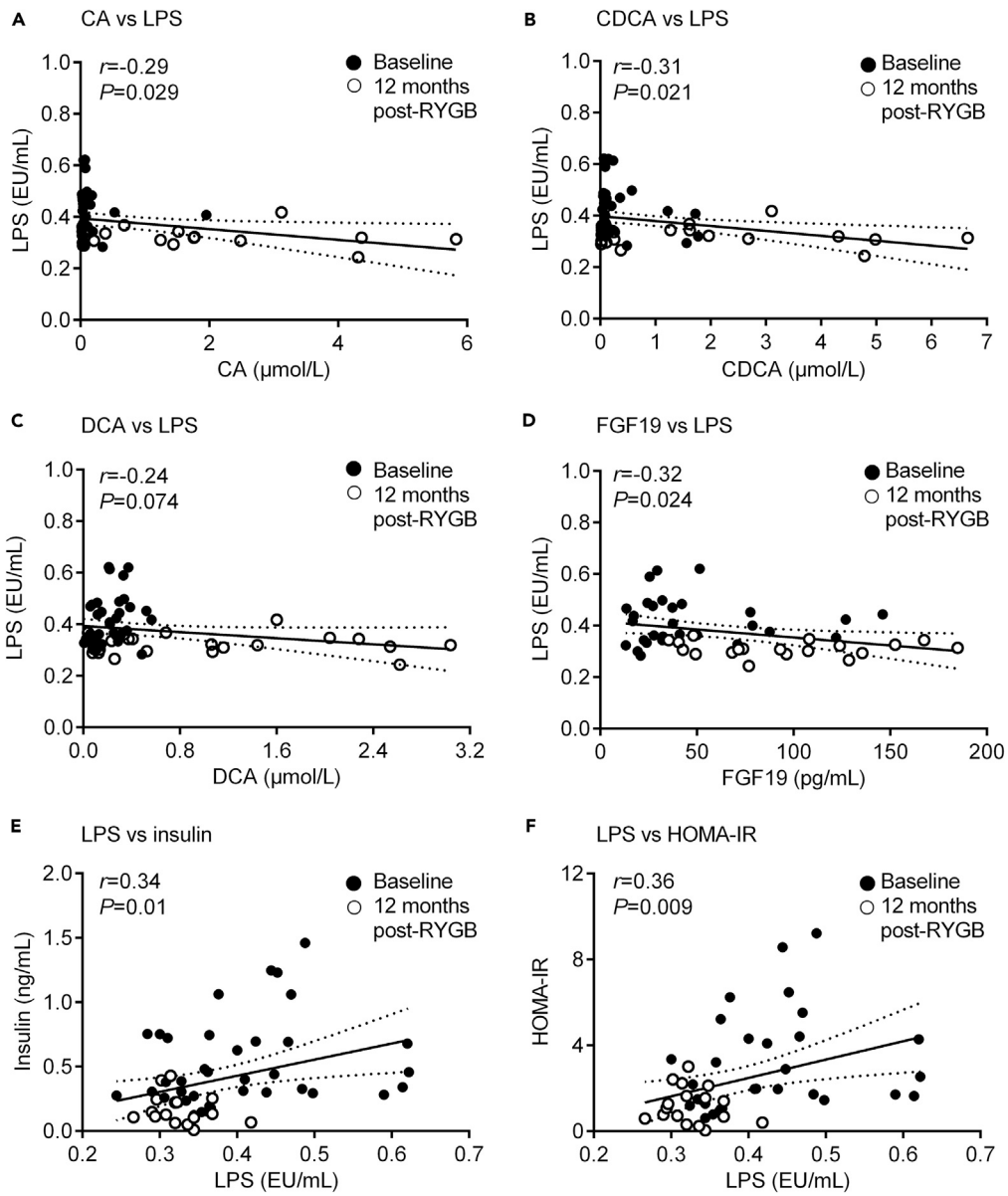

Figure 5. Plasma CA, CDCA, and FGF19 Levels Negatively Correlate with Endotoxemia Severity in Pre-Diabetic/Diabetic RYGB Patients

(A–D) Pearson correlations between fasting plasma CA (A), CDCA (B), DCA (C), and FGF19 (D) concentrations with fasting plasma LPS concentrations in RYGB patients at baseline (black circles; n = 31–34) and 12 months after surgery (white circles; n = 20–26).

(E and F) Pearson correlations between fasting plasma LPS concentrations with fasting plasma insulin concentrations (E) and HOMA-IR indices (F) in RYGB patients at baseline (black circles; n = 31–34) and 12 months after surgery (white circles; n = 20–26).

Solid regression lines indicate least squares fit of data and dashed lines indicate 95% confidence intervals. Statistical significance was determined by two-tailed, unpaired t test.

et al., 2013; Pournaras et al., 2012), RYGB almost tripled fasting plasma FGF19 levels (Table 2) indicating intestinal FXR activation. When merging the data from baseline and 12 months after RYGB (Mani et al., 2019), regression analysis additionally revealed that fasting plasma CA (Figure 5A), CDCA (Figure 5B), and FGF19 (Figure 5D) levels weakly, but significantly, negatively correlated with fasting plasma LPS levels, while DCA trended in the same direction (Figure 5C). Further, fasting plasma LPS levels positively correlated with fasting plasma insulin levels and HOMA-IR indices (Figures 5E and 5F).

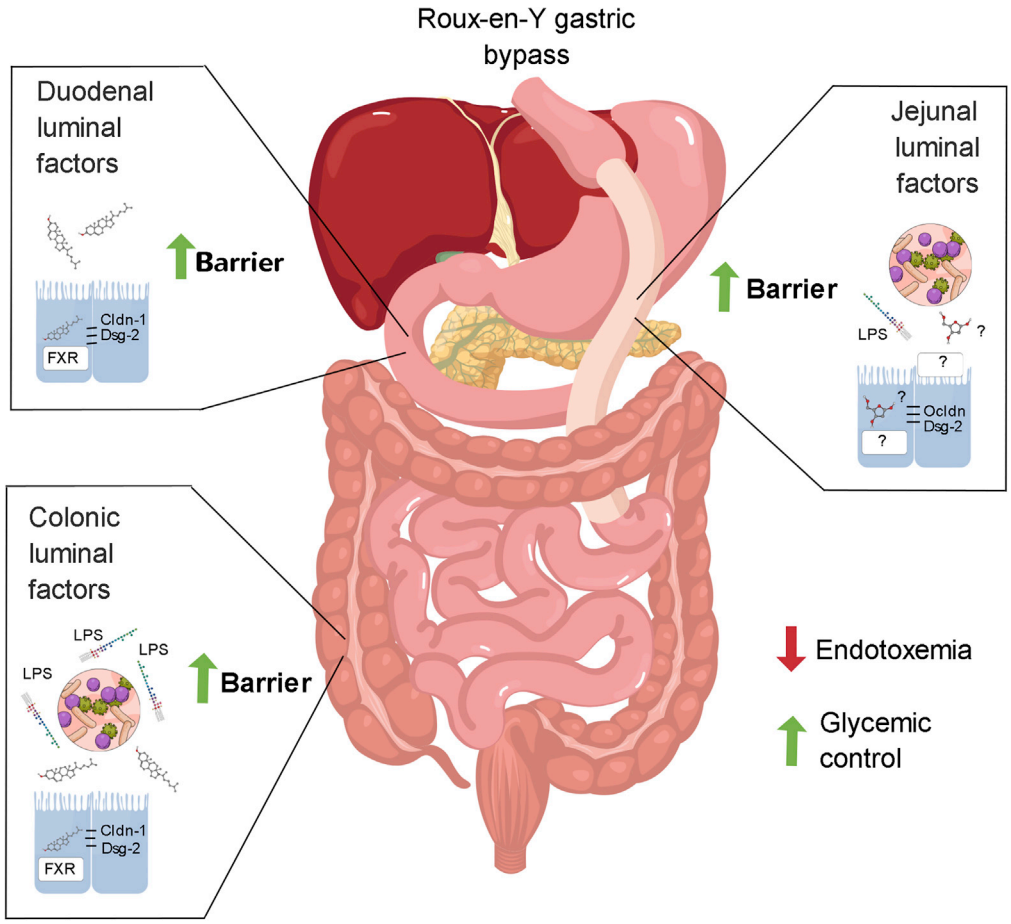

Figure 6. Region-Specific Mechanisms for Intestinal Luminal Factors in Stabilizing the Intestinal Epithelial Barrier following RYGB

Schematic diagram illustrating a proposed model based on the findings of the present study. While duodenal luminal factors following RYGB may locally stabilize the IEB partly through FXR, this would not be expected to have an overall impact on endotoxemia-induced insulin resistance and glycemic control due to the low bacterial load in the duodenal contents. However, colonic luminal factors following RYGB may locally stabilize the IEB partly through FXR to attenuate endotoxemia-induced insulin resistance and improve glycemic control due to the high bacterial load in the colonic contents. Similarly, jejunal luminal factors following RYGB may locally stabilize the IEB to attenuate endotoxemia-induced insulin resistance and improve glycemic control due to the moderate bacterial load in the jejunal contents, although this would be independent of FXR signaling possibly due to the redirection of bile flow away from the upper jejunum post-operatively.

DISCUSSION

The main objective of the present study was to gain mechanistic insight into how RYGB consistently stabilizes the IEB/attenuates endotoxemia across species (Guo et al., 2019; Monte et al., 2012; Steensels et al., 2017; Troseid et al., 2013; Wang et al., 2019a; Wu et al., 2019; Yang et al., 2014) in order to inform the design of more effective pharmacotherapies against insulin resistance and type 2 diabetes. We administered the intestinal contents of RYGB-operated and sham-operated rats to germ-free mice and Caco-2 cells. This unique approach led us to identify a close interaction between intestinal luminal factors with intestinal FXR signaling as a potential contributor to the stabilized IEB/attenuated endotoxemia following RYGB (Figure 6), which was corroborated in a longitudinal cohort of 38 pre-diabetic/diabetic patients.

We previously found that the cecal contents of RYGB-operated compared with sham-operated ZF rats conferred superior oral glucose tolerance to recipient germ-free mice (Arora et al., 2017). We have now extended these findings to include the jejunal and colonic contents of RYGB-operated compared with sham-operated diet-induced obese rats and have further provided an association with suppression of

endotoxemia. Interestingly, the blood glucose excursion curves of recipient germ-free mice in the present study suggest that the jejunal contents of RYGB-operated compared with sham-operated rats may mainly enhance insulin release, while the colonic contents may mainly enhance peripheral insulin sensitivity. Future glucose-stimulated insulin secretion assays and hyperinsulinaemic-euglycaemic clamp studies performed on recipient germ-free mice are needed to confirm this. In contrast, the lack of effect of the duodenal contents of RYGB-operated compared with sham-operated ZF rats on oral glucose tolerance in recipient germ-free mice is consistent with the low (gram-negative) bacterial load in this small intestinal region (Arora et al., 2017) and highlights the region-specific contribution of the gastrointestinal tract to regulating systemic endotoxemia (Chakaroun et al., 2020).

By applying the intestinal contents of RYGB-operated and sham-operated rats directly onto the apical side of Caco-2 cells, we partially simulated the regional intestinal microenvironments of the respective surgical groups. This revealed region-specific, barrier-stabilizing effects for the intestinal contents of RYGB-operated compared with sham-operated rats, possibly mediated by the action of various host- and/or microbiota-generated soluble factors. These potentially include, but are not limited to, hepatocyte-derived conjugated primary bile acids, that may become concentrated in the duodenum following RYGB due to redirection of ingested food passage to the mid-jejunum (Ise et al., 2019), as well as microbiota-derived metabolites such as indole-3-propionic acid (Jennis et al., 2018; Natividad et al., 2018), secondary bile acids (Haange et al., 2020; Lajczak-McGinley et al., 2020), taurine (Ahmadi et al., 2020; Wang et al., 2019a), and the short chain fatty acid propionate (Liou et al., 2013; Tong et al., 2016). Future metabolomics studies are required to confirm this, and to potentially discover novel soluble factors that stabilize the IEB.

Murine models of metabolic surgeries were originally developed to identify the molecular mediators behind their unique metabolic benefits using specific knockout lines (Stevenson et al., 2019). A landmark achievement using this approach is the identification of FXR and/or TGR5 as important molecular targets of VSG (Ding et al., 2016; McGavigan et al., 2017; Ryan et al., 2014), bile diversion to the ileum (BDI) (Albaugh et al., 2019; Pierre et al., 2019), and RYGB (Li et al., 2020). Remarkably, while mice deficient for FXR show normal changes in whole-body energy balance following RYGB, they do not present with fully improved oral glucose tolerance, insulin tolerance, and HOMA-IR indices (Li et al., 2020). The findings of the present study suggest that this could be due to persistently elevated endotoxemia post-operatively, possibly from the loss of intestinal FXR-mediated stabilization of the IEB, which can be formally assessed in mice lacking FXR specifically in enterocytes (Albaugh et al., 2019). In contrast, mice deficient for TGR5 respond normally to RYGB (Hao et al., 2018), which is in line with the lack of effect of TGR5 blockade on barrier function in Caco-2 cells in response to the intestinal contents of RYGB-operated rats reported here.

We could confirm the widely documented rise in various primary and secondary plasma bile acids in patients following RYGB (Ding et al., 2019). This may reflect increased intestinal luminal bile acid levels and organic anion-transporting peptide (OATP)-mediated re-uptake by enterocytes, as has been shown in rats following duodenal-jejunal bypass (Ueno et al., 2020), an experimental surgical procedure anatomically similar to RYGB. By extension, FXR could be activated in enterocytes to stabilize the IEB following RYGB in patients as proposed for rodents above. Indeed, we could link the post-operative rise in plasma FGF19 levels, a readout of intestinal FXR activation, to attenuated endotoxemia, which itself positively associated with HOMA-IR indices. However, it should be stressed that correlation does not prove causation. Future studies are required to confirm if the intestinal contents or at least the stool of patients following RYGB compared with baseline have FXR-mediated, barrier-stabilizing effects in enterocytes.

Limitations of the Study

We did not analyze intestinal microbiota in the present study so cannot exclude the possibility that the attenuated endotoxemia following RYGB is due to an overall reduction of intestinal LPS-producing, gram-negative bacteria. We think that this is unlikely however as we have previously shown that such intestinal bacteria, including *Bacteroides* species, are markedly increased throughout the gastrointestinal tract in RYGB-operated compared with sham-operated rats (Arora et al., 2017). Our *in vitro* system did not include intestinal immune cells, which could contribute to the stabilized IEB following RYGB (Luck et al., 2019; Wang et al., 2019a). Nevertheless, our approach using Caco-2 cells alone allowed us to establish direct, cell-autonomous roles for intestinal contents in regulating IEB function and structure. We could not employ pair-fed or body weight-matched groups in our rat experiments, so it is possible that the stabilized IEB/attenuated endotoxemia reported here are not specific to RYGB. However, previous findings

from diet-induced obese mice and rats, as well as genetically obese and insulin-resistant ZDF rats, have established that reduced intestinal permeability/attenuated endotoxemia following RYGB occur independently of food/high-fat diet restriction and weight loss (Guo et al., 2019; Steensels et al., 2017; Wang et al., 2019a). Additionally, we previously found that colonic CA and CDCA concentrations are twice as high in RYGB-operated, diet-induced obese rats compared with body weight-matched, sham-operated counterparts (Haange et al., 2020), further supporting the view that gastrointestinal reconfiguration-induced changes in bile flow and bile acid metabolizing intestinal microbiota *per se*, contribute to increased colonic FXR activation and stabilization of the IEB (Figure 6). This is also supported by the finding that the jejunal contents of RYGB-operated rats stabilized barrier function in Caco-2 cells independently of FXR, since bile flow is redirected away from the upper/mid jejunum post-operatively. Nevertheless, future bile acid measurements of the duodenal and colonic contents of RYGB-operated rats by nuclear magnetic resonance spectroscopy are needed to identify the precise molecular mechanisms responsible for their barrier-stabilizing effects, akin to that performed for mouse cecal contents in the context of enhanced enteroendocrine cell function following VSG (Chaudhari et al., 2020).

In summary, we have presented a combination of pre-clinical and clinical evidence suggesting that RYGB stabilizes the IEB potentially through a synergistic interaction between intestinal luminal factors and intestinal FXR signaling. Our findings also provide an experimental framework for identifying other signaling pathways in enterocytes responsible for attenuating endotoxemia following RYGB, which could be exploited for the more effective, non-invasive treatment of insulin resistance in obesity and possibly also other metabolic disorders.

Resource Availability

Lead Contact

Further information and requests for resources should be directed to and, where possible, will be fulfilled by the Lead Contact, Mohammed Hankir (hankir_m@ukw.de).

Materials Availability

All reagents used in this study will be made available on reasonable request to the Lead Contact.

Data and Code Availability

The original/source data are available from the Lead Contact on reasonable request.

METHODS

All methods can be found in the accompanying Transparent Methods supplemental file.

SUPPLEMENTAL INFORMATION

Supplemental Information can be found online at https://doi.org/10.1016/j.isci.2020.101777.

ACKNOWLEDGMENTS

This work was supported by the Interdisziplinäre Zentrum für Klinische Forschung (IZKF) Wuerzburg (Grant number IZKF Z-2/71) and the Deutsche Forschungsgemeinschaft (DFG) (grant number SCHL 1962/5-2). We thank Veronica Heimbach for excellent technical assistant with Caco-2 cells and Carina Rosenberg for excellent husbandry of germ-free mice.

AUTHOR CONTRIBUTIONS

Conceptualization: M.K.H., F.S., and N.S.; Methodology: M.K.H., M.K., M.K., T.A., F.S., and N.S.; Investigation: M.K.H., T.L., E.E.B., Y. G., M.K., M.K., U.D., C.O., C.L.W., T.A., and F.S.; Resources: E.E.B., M.K., M.K., T.A., F.S., and N.S.; Writing (initial draft) and data analysis: M.K.H., T.A., and N.S.; Funding Acquisition: F.S., U.D., and N.S.; Supervision: M.K.H. and N.S. All authors read and contributed to the final version of the manuscript.

DECLARATION OF INTERESTS

The authors declare no competing interests.

Received: September 14, 2020
Revised: October 12, 2020
Accepted: November 3, 2020
Published: December 18, 2020

REFERENCES

Adams, T.D., Davidson, L.E., Litwin, S.E., Kim, J., Kolotkin, R.L., Nanjee, M.N., Gutierrez, J.M., Frogley, S.J., Ibele, A.R., Brinton, E.A., et al. (2016). Weight and metabolic outcomes 12 Years after gastric bypass. N. Engl. J. Med. *377*, 1143–1155.

Ahlin, S., Cefalu, C., Bondia-Pons, I., Capristo, E., Marini, L., Gastaldelli, A., Mingrone, G., and Nolan, J.J. (2019). Bile acid changes after metabolic surgery are linked to improvement in insulin sensitivity. Br. J. Surg. *106*, 1178–1186.

Ahmadi, S., Wang, S., Nagpal, R., Wang, B., Jain, S., Razazan, A., Mishra, S.P., Zhu, X., Wang, Z., Kavanagh, K., et al. (2020). A human-origin probiotic cocktail ameliorates aging-related leaky gut and inflammation via modulating the microbiota/taurine/tight junction axis. JCI Insight *5*, e132055.

Albaugh, V.L., Banan, B., Antoun, J., Xiong, Y., Guo, Y., Ping, J., Alikhan, M., Clements, B.A., Abumrad, N.N., and Flynn, C.R. (2019). Role of bile acids and GLP-1 in mediating the metabolic improvements of bariatric surgery. Gastroenterology *156*, 1041–1051.

Albers, P.H., Bojsen-Moller, K.N., Dirksen, C., Serup, A.K., Kristensen, D.E., Frystyk, J., Clausen, T.R., Kiens, B., Richter, E.A., Madsbad, S., et al. (2015). Enhanced insulin signaling in human skeletal muscle and adipose tissue following gastric bypass surgery. Am. J. Physiol. Regul. Integr. Comp. Physiol. *309*, R510–R524.

Arora, T., Seyfried, F., Docherty, N.G., Tremaroli, V., le Roux, C.W., Perkins, R., and Backhed, F. (2017). Diabetes-associated microbiota in fa/fa rats is modified by Roux-en-Y gastric bypass. ISME J. *11*, 2035–2046.

Bankoglu, E.E., Arnold, C., Hering, I., Hankir, M., Seyfried, F., and Stopper, H. (2018). Decreased chromosomal damage in lymphocytes of obese patients after bariatric surgery. Sci. Rep. *8*, e11195.

Baud, G., Daoudi, M., Hubert, T., Raverdy, V., Pigeyre, M., Hervieux, E., Devienne, M., Ghunaim, M., Bonner, C., Quenon, A., et al. (2016). Bile diversion in roux-en-Y gastric bypass modulates sodium-dependent glucose intestinal uptake. Cell Metab. *23*, 547–553.

Bhutta, H.Y., Rajpal, N., White, W., Freudenberg, J.M., Liu, Y., Way, J., Rajpal, D., Cooper, D.C., Young, A., Tavakkoli, A., et al. (2015). Effect of Roux-en-Y gastric bypass surgery on bile acid metabolism in normal and obese diabetic rats. PLoS One *10*, e0122273.

Bikman, B.T., Zheng, D., Pories, W.J., Chapman, W., Pender, J.R., Bowden, R.C., Reed, M.A., Cortright, R.N., Tapscott, E.B., Houmard, J.A., et al. (2008). Mechanism for improved insulin sensitivity after gastric bypass surgery. J. Clin. Endocrinol. Metab. *93*, 4656–4663.

Bojsen-Moller, K.N., Dirksen, C., Jorgensen, N.B., Jacobsen, S.H., Serup, A.K., Albers, P.H., Hansen, D.L., Worm, D., Naver, L., Kristiansen, V.B., et al. (2014). Early enhancements of hepatic and later of peripheral insulin sensitivity combined with increased postprandial insulin secretion contribute to improved glycemic control after Roux-en-Y gastric bypass. Diabetes *63*, 1725–1737.

Campos, G.M., Rabl, C., Peeva, S., Ciovica, R., Rao, M., Schwarz, J.M., Havel, P., Schambelan, M., and Mulligan, K. (2010). Improvement in peripheral glucose uptake after gastric bypass surgery is observed only after substantial weight loss has occurred and correlates with the magnitude of weight lost. J. Gastrointest. Surg. *14*, 15–23.

Cani, P.D., Amar, J., Iglesias, M.A., Poggi, M., Knauf, C., Bastelica, D., Neyrinck, A.M., Fava, F., Tuohy, K.M., Chabo, C., et al. (2007). Metabolic endotoxemia initiates obesity and insulin resistance. Diabetes *56*, 1761–1772.

Cani, P.D., Bibiloni, R., Knauf, C., Waget, A., Neyrinck, A.M., Delzenne, N.M., and Burcelin, R. (2008). Changes in gut microbiota control metabolic endotoxemia-induced inflammation in high-fat diet-induced obesity and diabetes in mice. Diabetes *57*, 1470–1481.

Cavin, J.B., Couvelard, A., Lebtahi, R., Ducroc, R., Arapis, K., Voitellier, E., Cluzeaud, F., Gillard, L., Hourseau, M., Mikail, N., et al. (2016). Differences in alimentary glucose absorption and intestinal disposal of blood glucose after roux-en-Y gastric bypass vs sleeve gastrectomy. Gastroenterology *150*, 454–464.

Chakaroun, R.M., Massier, L., and Kovacs, P. (2020). Gut microbiome, intestinal permeability, and tissue bacteria in metabolic disease: perpetrators or bystanders? Nutrients *12*, e1082.

Chambers, A.P., Jessen, L., Ryan, K.K., Sisley, S., Wilson-Perez, H.E., Stefater, M.A., Gaitonde, S.G., Sorrell, J.E., Toure, M., Berger, J., et al. (2011). Weight-independent changes in blood glucose homeostasis after gastric bypass or vertical sleeve gastrectomy in rats. Gastroenterology *141*, 950–958.

Chaudhari, S.N., Harris, D.A., Aliakbarian, H., Luo, J.N., Henke, M.T., Subramaniam, R., Vernon, A.H., Tavakkoli, A., Sheu, E.G., and Devlin, A.S. (2020). Bariatric surgery reveals a gut-restricted TGR5 agonist with anti-diabetic effects. Nat. Chem. Biol. https://doi.org/10.1038/s41589-020-0604-z.

Chen, Y., Lu, J., Nemati, R., Plank, L.D., and Murphy, R. (2019). Acute changes of bile acids and FGF19 after sleeve gastrectomy and roux-en-Y gastric bypass. Obes. Surg. *29*, 3605–3621.

Cheng, K.C., Chang, W.T., Kuo, F.Y., Chen, Z.C., Li, Y., and Cheng, J.T. (2019). TGR5 activation ameliorates hyperglycemia-induced cardiac hypertrophy in H9c2 cells. Sci. Rep. *9*, e3633.

Cipriani, S., Mencarelli, A., Chini, M.G., Distrutti, E., Renga, B., Bifulco, G., Baldelli, F., Donini, A., and Fiorucci, S. (2011). The bile acid receptor GPBAR-1 (TGR5) modulates integrity of intestinal barrier and immune response to experimental colitis. PLoS One *6*, e25637.

DePaoli, A.M., Zhou, M., Kaplan, D.D., Hunt, S.C., Adams, T.D., Learned, R.M., Tian, H., and Ling, L. (2019). FGF19 analog as a surgical factor mimetic that contributes to metabolic effects beyond glucose homeostasis. Diabetes *68*, 1315–1328.

Depommier, C., Everard, A., Druart, C., Plovier, H., Van Hul, M., Vieira-Silva, S., Falony, G., Raes, J., Maiter, D., Delzenne, N.M., et al. (2019). Supplementation with Akkermansia muciniphila in overweight and obese human volunteers: a proof-of-concept exploratory study. Nat. Med. *25*, 1096–1103.

Ding, L., Fang, Z., Liu, Y., Zhang, E., Huang, T., Yang, L., Wang, Z., and Huang, W. (2019). Targeting bile acid-activated receptors in bariatric surgery. Handb. Exp. Pharmacol. *256*, 359–378.

Ding, L., Sousa, K.M., Jin, L., Dong, B., Kim, B.W., Ramirez, R., Xiao, Z., Gu, Y., Yang, Q., Wang, J., et al. (2016). Vertical sleeve gastrectomy activates GPBAR-1/TGR5 to sustain weight loss, improve fatty liver, and remit insulin resistance in mice. Hepatology *64*, 760–773.

Dischinger, U., Corteville, C., Otto, C., Fassnacht, M., Seyfried, F., and Hankir, M.K. (2019). GLP-1 and PYY3-36 reduce high-fat food preference additively after Roux-en-Y gastric bypass in diet-induced obese rats. Surg. Obes. Relat. Dis. *15*, 1483–1492.

Evans, K.A., Budzik, B.W., Ross, S.A., Wisnoski, D.D., Jin, J., Rivero, R.A., Vimal, M., Szewczyk, G.R., Jayawickreme, C., Moncol, D.L., et al. (2009). Discovery of 3-aryl-4-isoxazolecarboxamides as TGR5 receptor agonists. J. Med. Chem. *52*, 7962–7965.

Fang, S., Suh, J.M., Reilly, S.M., Yu, E., Osborn, O., Lackey, D., Yoshihara, E., Perino, A., Jacinto, S., Lukasheva, Y., et al. (2015). Intestinal FXR agonism promotes adipose tissue browning and reduces obesity and insulin resistance. Nat. Med. *21*, 159–165.

Ferrannini, E., Camastra, S., Astiarraga, B., Nannipieri, M., Castro-Perez, J., Xie, D., Wang, L., Chakravarthy, M., and Haeusler, R.A. (2015). Increased bile acid synthesis and deconjugation after biliopancreatic diversion. Diabetes *64*, 3377–3385.

Flatt, B., Martin, R., Wang, T.L., Mahaney, P., Murphy, B., Gu, X.H., Foster, P., Li, J., Pircher, P., Petrowski, M., et al. (2009). Discovery of XL335 (WAY-362450), a highly potent, selective, and

orally active agonist of the farnesoid X receptor (FXR). J. Med. Chem. *52*, 904–907.

Gancheva, S., Ouni, M., Jelenik, T., Koliaki, C., Szendroedi, J., Toledo, F.G.S., Markgraf, D.F., Pesta, D.H., Mastrototaro, L., De Filippo, E., et al. (2019). Dynamic changes of muscle insulin sensitivity after metabolic surgery. Nat. Commun. *10*, e4179.

Garcia-Hernandez, V., Quiros, M., and Nusrat, A. (2017). Intestinal epithelial claudins: expression and regulation in homeostasis and inflammation. Ann. N. Y. Acad. Sci. *1397*, 66–79.

Garcia, M.A., Nelson, W.J., and Chavez, N. (2018). Cell-cell junctions organize structural and signaling networks. Cold Spring Harb. Perspect. Biol. *10*, a029181.

Gerhard, G.S., Styer, A.M., Wood, G.C., Roesch, S.L., Petrick, A.T., Gabrielsen, J., Strodel, W.E., Still, C.D., and Argyropoulos, G. (2013). A role for fibroblast growth factor 19 and bile acids in diabetes remission after Roux-en-Y gastric bypass. Diabetes Care *36*, 1859–1864.

Guerville, M., Leroy, A., Sinquin, A., Laugerette, F., Michalski, M.C., and Boudry, G. (2017). Western-diet consumption induces alteration of barrier function mechanisms in the ileum that correlates with metabolic endotoxemia in rats. Am. J. Physiol. Endocrinol. Metab. *313*, E107–E120.

Guida, C., Stephen, S.D., Watson, M., Dempster, N., Larraufie, P., Marjot, T., Cargill, T., Rickers, L., Pavlides, M., Tomlinson, J., et al. (2019). PYY plays a key role in the resolution of diabetes following bariatric surgery in humans. EBioMedicine *40*, 67–76.

Guo, Y., Liu, C.Q., Liu, G.P., Huang, Z.P., and Zou, D.J. (2019). Roux-en-Y gastric bypass decreases endotoxemia and inflammatory stress in association with improvements in gut permeability in obese diabetic rats. J. Diabetes *11*, 786–793.

Haange, S.B., Jehmlich, N., Krugel, U., Hintschich, C., Wehrmann, D., Hankir, M., Seyfried, F., Froment, J., Hubschmann, T., Muller, S., et al. (2020). Gastric bypass surgery in a rat model alters the community structure and functional composition of the intestinal microbiota independently of weight loss. Microbiome *8*, 13.

Hankir, M.K., Seyfried, F., Hintschich, C.A., Diep, T.A., Kleberg, K., Kranz, M., Deuther-Conrad, W., Tellez, L.A., Rullmann, M., Patt, M., et al. (2017). Gastric bypass surgery recruits a gut PPAR-alpha-striatal D1R pathway to reduce fat appetite in obese rats. Cell Metab. *25*, 335–344.

Hao, Z., Leigh Townsend, R., Mumphrey, M.B., Gettys, T.W., Yu, S., Munzberg, H., Morrison, C.D., and Berthoud, H.R. (2018). Roux-en-Y gastric bypass surgery-induced weight loss and metabolic improvements are similar in TGR5-deficient and wildtype mice. Obes. Surg. *28*, 3227–3236.

Hartmann, P., Hochrath, K., Horvath, A., Chen, P., Seebauer, C.T., Llorente, C., Wang, L., Alnouti, Y., Fouts, D.E., Starkel, P., et al. (2018). Modulation of the intestinal bile acid/farnesoid X receptor/fibroblast growth factor 15 axis improves alcoholic liver disease in mice. Hepatology *67*, 2150–2166.

He, B., Chen, L., Yu, C., Piao, D., Wang, Y., and Han, P. (2014). Roux-en-Y gastric bypass increases hepatic and peripheral insulin sensitivity in rats with type 2 diabetes mellitus. Surg. Obes. Relat. Dis. *10*, 485–493.

Heinemann, U., and Schuetz, A. (2019). Structural features of tight-junction proteins. Int. J. Mol. Sci. *20*, e6020.

Illan-Gomez, F., Gonzalvez-Ortega, M., Orea-Soler, I., Alcaraz-Tafalla, M.S., Aragon-Alonso, A., Pascual-Diaz, M., Perez-Paredes, M., and Lozano-Almela, M.L. (2012). Obesity and inflammation: change in adiponectin, C-reactive protein, tumour necrosis factor-alpha and interleukin-6 after bariatric surgery. Obes. Surg. *22*, 950–955.

Inagaki, T., Choi, M., Moschetta, A., Peng, L., Cummins, C.L., McDonald, J.G., Luo, G., Jones, S.A., Goodwin, B., Richardson, J.A., et al. (2005a). Fibroblast growth factor 15 functions as an enterohepatic signal to regulate bile acid homeostasis. Cell Metab. *2*, 217–225.

Inagaki, T., Moschetta, A., Lee, Y.K., Peng, L., Zhao, G., Downes, M., Yu, R.T., Shelton, J.M., Richardson, J.A., Repa, J.J., et al. (2005b). Regulation of antibacterial defense in the small intestine by the nuclear bile acid receptor. Proc. Natl. Acad. Sci. U S A *103*, 3920–3925.

Ise, I., Tanaka, N., Imoto, H., Maekawa, M., Kohyama, A., Watanabe, K., Motoi, F., Unno, M., and Naitoh, T. (2019). Changes in enterohepatic circulation after duodenal-jejunal bypass and reabsorption of bile acids in the bilio-pancreatic limb. Obes. Surg. *29*, 1901–1910.

Jennis, M., Cavanaugh, C.R., Leo, G.C., Mabus, J.R., Lenhard, J., and Hornby, P.J. (2018). Microbiota-derived tryptophan indoles increase after gastric bypass surgery and reduce intestinal permeability in vitro and in vivo. Neurogastroenterol. Motil. *30*, e13178.

Jorgensen, N.B., Dirksen, C., Bojsen-Moller, K.N., Jacobsen, S.H., Worm, D., Hansen, D.L., Kristiansen, V.B., Naver, L., Madsbad, S., and Holst, J.J. (2013). Exaggerated glucagon-like peptide 1 response is important for improved beta-cell function and glucose tolerance after Roux-en-Y gastric bypass in patients with type 2 diabetes. Diabetes *62*, 3044–3052.

Kohli, R., Bradley, D., Setchell, K.D., Eagon, J.C., Abumrad, N., and Klein, S. (2013). Weight loss induced by Roux-en-Y gastric bypass but not laparoscopic adjustable gastric banding increases circulating bile acids. J. Clin. Endocrinol. Metab. *98*, E708–E712.

Laferrere, B., Reilly, D., Arias, S., Swerdlow, N., Gorroochurn, P., Bawa, B., Bose, M., Teixeira, J., Stevens, R.D., Wenner, B.R., et al. (2011). Differential metabolic impact of gastric bypass surgery versus dietary intervention in obese diabetic subjects despite identical weight loss. Sci. Transl. Med. *3*, 80re82.

Lajczak-McGinley, N.K., Porru, E., Fallon, C.M., Smyth, J., Curley, C., McCarron, P.A., Tambuwala, M.M., Roda, A., and Keely, S.J. (2020). The secondary bile acids, ursodeoxycholic acid and lithocholic acid, protect against intestinal inflammation by inhibition of epithelial apoptosis. Physiol. Rep. *8*, e14456.

Lea, T. (2015). Caco-2 Cell Line. In The Impact of Food Bioactives on Health: In Vitro and Ex Vivo Models, Kitty Verhoeckx, ed. (Springer), pp. 103–112, Chapter 10.

Li, K., Zou, J., Li, S., Guo, J., Shi, W., Wang, B., Han, X., Zhang, H., Zhang, P., Miao, Z., et al. (2020). Farnesoid X receptor contributes to body weight-independent improvements in glycemic control after Roux-en-Y gastric bypass surgery in diet-induced obese mice. Mol. Metab. *37*, 100980.

Li, Y., Cheng, K.C., Niu, C.S., Lo, S.H., Cheng, J.T., and Niu, H.S. (2017). Investigation of triamterene as an inhibitor of the TGR5 receptor: identification in cells and animals. Drug Des. Devel. Ther. *11*, 1127–1134.

Li, Z., Hardij, J., Evers, S.S., Hutch, C.R., Choi, S.M., Shao, Y., Learman, B.S., Lewis, K.T., Schill, R.L., Mori, H., et al. (2019). G-CSF partially mediates effects of sleeve gastrectomy on the bone marrow niche. J. Clin. Invest. *129*, 2404–2416.

Lima, M.M., Pareja, J.C., Alegre, S.M., Geloneze, S.R., Kahn, S.E., Astiarraga, B.D., Chaim, E.A., and Geloneze, B. (2010). Acute effect of roux-en-y gastric bypass on whole-body insulin sensitivity: a study with the euglycemic-hyperinsulinemic clamp. J. Clin. Endocrinol. Metab. *95*, 3871–3875.

Lin, Y.H., Luck, H., Khan, S., Schneeberger, P.H.H., Tsai, S., Clemente-Casares, X., Lei, H., Leu, Y.L., Chan, Y.T., Chen, H.Y., et al. (2019). Aryl hydrocarbon receptor agonist indigo protects against obesity-related insulin resistance through modulation of intestinal and metabolic tissue immunity. Int. J. Obes. *43*, 2407–2421.

Liou, A.P., Paziuk, M., Luevano, J.M., Jr., Machineni, S., Turnbaugh, P.J., and Kaplan, L.M. (2013). Conserved shifts in the gut microbiota due to gastric bypass reduce host weight and adiposity. Sci. Transl. Med. *5*, 178ra141.

Lips, M.A., Van Klinken, J.B., van Harmelen, V., Dharuri, H.K., t Hoen, P.A., Laros, J.F., van Ommen, G.J., Janssen, I.M., Van Ramshorst, B., Van Wagensveld, B.A., et al. (2014). Roux-en-Y gastric bypass surgery, but not calorie restriction, reduces plasma branched-chain amino acids in obese women independent of weight loss or the presence of type 2 diabetes. Diabetes Care *37*, 3150–3156.

Lo, S.H., Li, Y., Cheng, K.C., Niu, C.S., Cheng, J.T., and Niu, H.S. (2017). Ursolic acid activates the TGR5 receptor to enhance GLP-1 secretion in type 1-like diabetic rats. Naunyn Schmiedebergs Arch. Pharmacol. *390*, 1097–1104.

Luck, H., Khan, S., Kim, J.H., Copeland, J.K., Revelo, X.S., Tsai, S., Chakraborty, M., Cheng, K., Tao Chan, Y., Nohr, M.K., et al. (2019). Gut-associated IgA(+) immune cells regulate obesity-related insulin resistance. Nat. Commun. *10*, 3650.

Luck, H., Tsai, S., Chung, J., Clemente-Casares, X., Ghazarian, M., Revelo, X.S., Lei, H., Luk, C.T., Shi, S.Y., Surendra, A., et al. (2015). Regulation of obesity-related insulin resistance with gut anti-inflammatory agents. Cell Metab. *21*, 527–542.

Makinen, J., Hannukainen, J.C., Karmi, A., Immonen, H.M., Soinio, M., Nelimarkka, L., Savisto, N., Helmio, M., Ovaska, J., Salminen, P.,

et al. (2015). Obesity-associated intestinal insulin resistance is ameliorated after bariatric surgery. Diabetologia *58*, 1055–1062.

Mani, B.K., Puzziferri, N., He, Z., Rodriguez, J.A., Osborne-Lawrence, S., Metzger, N.P., Chhina, N., Gaylinn, B., Thorner, M.O., Thomas, E.L., et al. (2019). LEAP2 changes with body mass and food intake in humans and mice. J. Clin. Invest. *129*, 3909–3923.

Martinussen, C., Bojsen-Moller, K.N., Dirksen, C., Jacobsen, S.H., Jorgensen, N.B., Kristiansen, V.B., Holst, J.J., and Madsbad, S. (2015). Immediate enhancement of first-phase insulin secretion and unchanged glucose effectiveness in patients with type 2 diabetes after Roux-en-Y gastric bypass. Am. J. Physiol. Endocrinol. Metab. *308*, E535–E544.

McGavigan, A.K., Garibay, D., Henseler, Z.M., Chen, J., Bettaieb, A., Haj, F.G., Ley, R.E., Chouinard, M.L., and Cummings, B.P. (2017). TGR5 contributes to glucoregulatory improvements after vertical sleeve gastrectomy in mice. Gut *66*, 226–234.

Meir, M., Salm, J., Fey, C., Schweinlin, M., Kollmann, C., Kannapin, F., Germer, C.T., Waschke, J., Beck, C., Burkard, N., et al. (2020). Enteroids generated from patients with severe inflammation in Crohn's disease maintain alterations of junctional proteins. J. Crohns Colitis *14*, 1473–1487.

Meirelles, K., Ahmed, T., Culnan, D.M., Lynch, C.J., Lang, C.H., and Cooney, R.N. (2009). Mechanisms of glucose homeostasis after Roux-en-Y gastric bypass surgery in the obese, insulin-resistant Zucker rat. Ann. Surg. *249*, 277–285.

Mingrone, G., Panunzi, S., De Gaetano, A., Guidone, C., Iaconelli, A., Leccesi, L., Nanni, G., Pomp, A., Castagneto, M., Ghirlanda, G., et al. (2012). Bariatric surgery versus conventional medical therapy for type 2 diabetes. N. Engl. J. Med. *366*, 1577–1585.

Mingrone, G., Panunzi, S., De Gaetano, A., Guidone, C., Iaconelli, A., Nanni, G., Castagneto, M., Bornstein, S., and Rubino, F. (2015). Bariatric-metabolic surgery versus conventional medical treatment in obese patients with type 2 diabetes: 5 year follow-up of an open-label, single-centre, randomised controlled trial. Lancet *386*, 964–973.

Monte, S.V., Caruana, J.A., Ghanim, H., Sia, C.L., Korzeniewski, K., Schentag, J.J., and Dandona, P. (2012). Reduction in endotoxemia, oxidative and inflammatory stress, and insulin resistance after Roux-en-Y gastric bypass surgery in patients with morbid obesity and type 2 diabetes mellitus. Surgery *151*, 587–593.

Moreno-Navarrete, J.M., Ortega, F., Serino, M., Luche, E., Waget, A., Pardo, G., Salvador, J., Ricart, W., Fruhbeck, G., Burcelin, R., et al. (2012). Circulating lipopolysaccharide-binding protein (LBP) as a marker of obesity-related insulin resistance. Int. J. Obes. *36*, 1442–1449.

Natividad, J.M., Agus, A., Planchais, J., Lamas, B., Jarry, A.C., Martin, R., Michel, M.L., Chong-Nguyen, C., Roussel, R., Straube, M., et al. (2018). Impaired aryl hydrocarbon receptor ligand production by the gut microbiota is a key factor in metabolic syndrome. Cell Metab. *28*, 737–749.

Pal, A., Rhoads, D.B., and Tavakkoli, A. (2019). Portal milieu and the interplay of multiple antidiabetic effects after gastric bypass surgery. Am. J. Physiol. Gastrointest. Liver Physiol. *316*, G668–G678.

Panunzi, S., Carlsson, L., De Gaetano, A., Peltonen, M., Rice, T., Sjostrom, L., Mingrone, G., and Dixon, J.B. (2016). Determinants of diabetes remission and glycemic control after bariatric surgery. Diabetes Care *39*, 166–174.

Parks, D.J., Blanchard, S.G., Bledsoe, R.K., Chandra, G., Consler, T.G., Kliewer, S.A., Stimmel, J.B., Willson, T.M., Zavacki, A.M., Moore, D.D., et al. (1999). Bile acids: natural ligands for an orphan nuclear receptor. Science *284*, 1365–1368.

Pierre, J.F., Li, Y., Gomes, C.K., Rao, P., Chang, E.B., and Yin, D.P. (2019). Bile diversion improves metabolic phenotype dependent on farnesoid X receptor (FXR). Obesity *27*, 803–812.

Pournaras, D.J., Glicksman, C., Vincent, R.P., Kuganolipava, S., Alaghband-Zadeh, J., Mahon, D., Bekker, J.H., Ghatei, M.A., Bloom, S.R., Walters, J.R., et al. (2012). The role of bile after Roux-en-Y gastric bypass in promoting weight loss and improving glycaemic control. Endocrinology *153*, 3613–3619.

Ramracheya, R.D., McCulloch, L.J., Clark, A., Wiggins, D., Johannessen, H., Olsen, M.K., Cai, X., Zhao, C.M., Chen, D., and Rorsman, P. (2016). PYY-dependent restoration of impaired insulin and glucagon secretion in type 2 diabetes following roux-en-Y gastric bypass surgery. Cell Rep. *15*, 944–950.

Ruban, A., Stoenchev, K., Ashrafian, H., and Teare, J. (2019). Current treatments for obesity. Clin. Med. *19*, 205–212.

Ryan, K.K., Tremaroli, V., Clemmensen, C., Kovatcheva-Datchary, P., Myronovych, A., Karns, R., Wilson-Perez, H.E., Sandoval, D.A., Kohli, R., Backhed, F., et al. (2014). FXR is a molecular target for the effects of vertical sleeve gastrectomy. Nature *509*, 183–188.

Saeidi, N., Meoli, L., Nestoridi, E., Gupta, N.K., Kvas, S., Kucharczyk, J., Bonab, A.A., Fischman, A.J., Yarmush, M.L., and Stylopoulos, N. (2013). Reprogramming of intestinal glucose metabolism and glycemic control in rats after gastric bypass. Science *341*, 406–410.

Salehi, M., Gastaldelli, A., and D'Alessio, D.A. (2014). Blockade of glucagon-like peptide 1 receptor corrects postprandial hypoglycemia after gastric bypass. Gastroenterology *146*, 669–680.

Schlegel, N., Boerner, K., and Waschke, J. (2020). Targeting desmosomal adhesion and signalling for intestinal barrier stabilization in inflammatory bowel diseases-Lessons from experimental models and patients. Acta Physiol. *18*, e13492.

Sjostrom, L., Lindroos, A.K., Peltonen, M., Torgerson, J., Bouchard, C., Carlsson, B., Dahlgren, S., Larsson, B., Narbro, K., Sjostrom, C.D., et al. (2004). Lifestyle, diabetes, and cardiovascular risk factors 10 years after bariatric surgery. N. Engl. J. Med. *351*, 2683–2693.

Sjostrom, L., Narbro, K., Sjostrom, C.D., Karason, K., Larsson, B., Wedel, H., Lystig, T., Sullivan, M., Bouchard, C., Carlsson, B., et al. (2007). Effects of bariatric surgery on mortality in Swedish obese subjects. N. Engl. J. Med. *357*, 741–752.

Sorribas, M., Jakob, M.O., Yilmaz, B., Li, H., Stutz, D., Noser, Y., de Gottardi, A., Moghadamrad, S., Hassan, M., Albillos, A., et al. (2019). FxR-modulates the gut-vascular barrier by regulating the entry sites for bacterial translocation in experimental cirrhosis. J. Hepatol. *71*, 1126–1140.

Spinelli, V., Lalloyer, F., Baud, G., Osto, E., Kouach, M., Daoudi, M., Vallez, E., Raverdy, V., Goossens, J.F., Descat, A., et al. (2016). Influence of Roux-en-Y gastric bypass on plasma bile acid profiles: a comparative study between rats, pigs and humans. Int. J. Obes. *40*, 1260–1267.

Stearns, A.T., Balakrishnan, A., and Tavakkolizadeh, A. (2009). Impact of Roux-en-Y gastric bypass surgery on rat intestinal glucose transport. Am. J. Physiol. Gastrointest. Liver Physiol. *297*, G950–G957.

Steensels, S., Lannoo, M., Avau, B., Laermans, J., Vancleef, L., Farre, R., Verbeke, K., and Depoortere, I. (2017). The role of nutrient sensing in the metabolic changes after gastric bypass surgery. J. Endocrinol. *232*, 363–376.

Steven, S., Hollingsworth, K.G., Small, P.K., Woodcock, S.A., Pucci, A., Aribasala, B., Al-Mrabeh, A., Batterham, R.L., and Taylor, R. (2016). Calorie restriction and not glucagon-like peptide-1 explains the acute improvement in glucose control after gastric bypass in Type 2 diabetes. Diabet. Med. *33*, 1723–1731.

Stevenson, M., Lee, J., Lau, R.G., Brathwaite, C.E.M., and Ragolia, L. (2019). Surgical mouse models of vertical sleeve gastrectomy and roux-en Y gastric bypass: a review. Obes. Surg. *29*, 4084–4094.

Tong, L.C., Wang, Y., Wang, Z.B., Liu, W.Y., Sun, S., Li, L., Su, D.F., and Zhang, L.C. (2016). Propionate ameliorates dextran sodium sulfate-induced colitis by improving intestinal barrier function and reducing inflammation and oxidative stress. Front. Pharmacol. *7*, 253.

Tremaroli, V., Karlsson, F., Werling, M., Stahlman, M., Kovatcheva-Datchary, P., Olbers, T., Fandriks, L., le Roux, C.W., Nielsen, J., and Backhed, F. (2015). Roux-en-Y gastric bypass and vertical banded gastroplasty induce long-term changes on the human gut microbiome contributing to fat mass regulation. Cell Metab. *22*, 228–238.

Troseid, M., Nestvold, T.K., Rudi, K., Thoresen, H., Nielsen, E.W., and Lappegard, K.T. (2013). Plasma lipopolysaccharide is closely associated with glycemic control and abdominal obesity: evidence from bariatric surgery. Diabetes Care *36*, 3627–3632.

Ueno, T., Tanaka, N., Imoto, H., Maekawa, M., Kohyama, A., Watanabe, K., Motoi, F., Kamei, T., Unno, M., and Naitoh, T. (2020). Mechanism of bile acid reabsorption in the biliopancreatic limb after duodenal-jejunal bypass in rats. Obes. Surg. *30*, 2528–2537.

Vancamelbeke, M., and Vermeire, S. (2017). The intestinal barrier: a fundamental role in health and disease. Expert Rev. Gastroenterol. Hepatol. *11*, 821–834.

Verbeke, L., Farre, R., Verbinnen, B., Covens, K., Vanuytsel, T., Verhaegen, J., Komuta, M., Roskams, T., Chatterjee, S., Annaert, P., et al. (2015). The FXR agonist obeticholic acid prevents gut barrier dysfunction and bacterial translocation in cholestatic rats. Am. J. Pathol. *185*, 409–419.

Viana, E.C., Araujo-Dasilio, K.L., Miguel, G.P., Bressan, J., Lemos, E.M., Moyses, M.R., de Abreu, G.R., de Azevedo, J.L., Carvalho, P.S., Passos-Bueno, M.R., et al. (2013). Gastric bypass and sleeve gastrectomy: the same impact on IL-6 and TNF-alpha. Prospective clinical trial. Obes. Surg. *23*, 1252–1261.

Wang, H., Chen, J., Hollister, K., Sowers, L.C., and Forman, B.M. (1999). Endogenous bile acids are ligands for the nuclear receptor FXR/BAR. Mol. Cell *3*, 543–553.

Wang, G., Wang, Q., Bai, J., Zhao, N., Wang, Y., Zhou, R., Kong, W., Zeng, T., Tao, K., and Xia, Z. (2019a). Upregulation of intestinal NLRP6 inflammasomes after roux-en-Y gastric bypass promotes gut immune homeostasis. Obes. Surg. *30*, 2528–2537.

Wang, K., Liao, M., Zhou, N., Bao, L., Ma, K., Zheng, Z., Wang, Y., Liu, C., Wang, W., Wang, J., et al. (2019b). Parabacteroides distasonis alleviates obesity and metabolic dysfunctions via production of succinate and secondary bile acids. Cell Rep. *26*, 222–235. e5.

Wang, L.Y., Cheng, K.C., Li, Y., Niu, C.S., Cheng, J.T., and Niu, H.S. (2017a). The dietary furocoumarin imperatorin increases plasma GLP-1 levels in type 1-like diabetic rats. Nutrients *9*, 1192.

Wang, L.Y., Cheng, K.C., Li, Y., Niu, C.S., Cheng, J.T., and Niu, H.S. (2017b). Glycyrrhizic acid increases glucagon like peptide-1 secretion via TGR5 activation in type 1-like diabetic rats. Biomed. Pharmacother. *95*, 599–604.

Wu, J., Zhang, P.B., Ren, Z.Q., Zhou, F., Hu, H.H., Zhang, H., Xue, K.K., Xu, P., and Shao, X.Q. (2019). Changes of serum lipopolysaccharide, inflammatory factors, and cecal microbiota in obese rats with type 2 diabetes induced by Roux-en-Y gastric bypass. Nutrition *67-68*, 110565.

Yan, Y., Sha, Y., Huang, X., Yuan, W., Wu, F., Hong, J., Fang, S., Huang, B., Hu, C., Wang, B., et al. (2019). Roux-en-Y gastric bypass improves metabolic conditions in association with increased serum bile acids level and hepatic farnesoid X receptor expression in a T2DM rat model. Obes. Surg. *29*, 2912–2922.

Yang, P.J., Lee, W.J., Tseng, P.H., Lee, P.H., Lin, M.T., and Yang, W.S. (2014). Bariatric surgery decreased the serum level of an endotoxin-associated marker: lipopolysaccharide-binding protein. Surg. Obes. Relat. Dis. *10*, 1182–1187.

Yoshino, M., Kayser, B.D., Yoshino, J., Stein, R.I., Reeds, D., Eagon, J.C., Eckhouse, S.R., Watrous, J.D., Jain, M., Knight, R., et al. (2020). Effects of diet versus gastric bypass on metabolic function in diabetes. N. Engl. J. Med. *383*, 721–732.

Yu, D.D., Lin, W., Forman, B.M., and Chen, T. (2014). Identification of trisubstituted-pyrazol carboxamide analogs as novel and potent antagonists of farnesoid X receptor. Bioorg. Med. Chem. *22*, 2919–2938.

Zhai, H., Li, Z., Peng, M., Huang, Z., Qin, T., Chen, L., Li, H., Zhang, H., Zhang, W., and Xu, G. (2018). Takeda G protein-coupled receptor 5-mechanistic target of rapamycin complex 1 signaling contributes to the increment of glucagon-like peptide-1 production after roux-en-Y gastric bypass. EBioMedicine *32*, 201–214.

iScience, Volume *23*

Supplemental Information

Simulating the Post-gastric Bypass Intestinal Microenvironment Uncovers a Barrier-Stabilizing Role for FXR

Mohammed K. Hankir, Theresa Langseder, Ezgi Eyluel Bankoglu, Yalda Ghoreishi, Ulrich Dischinger, Max Kurlbaum, Matthias Kroiss, Christoph Otto, Carel W. le Roux, Tulika Arora, Florian Seyfried, and Nicolas Schlegel

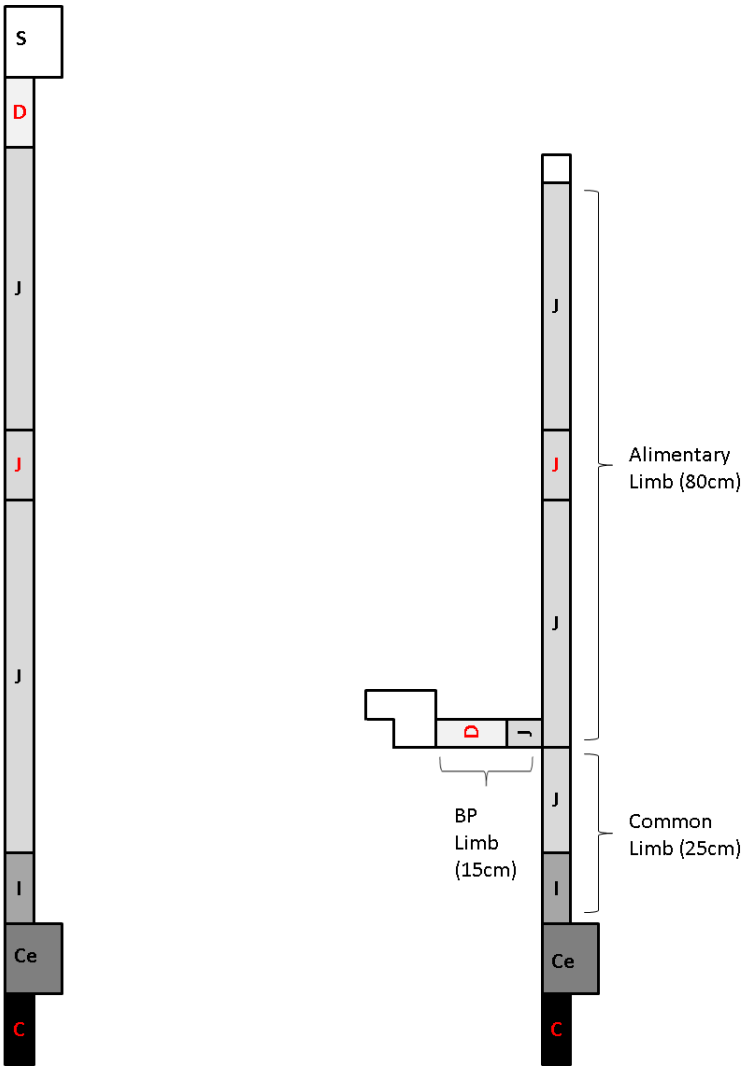

Figure S1. Schematic Diagram Showing Sham (Left) and RYGB (Right) Rat Gastrointestinal Anatomies and Intestinal Contents Sampling Sites (Highlighted in Red Text), Related to Figure 1.

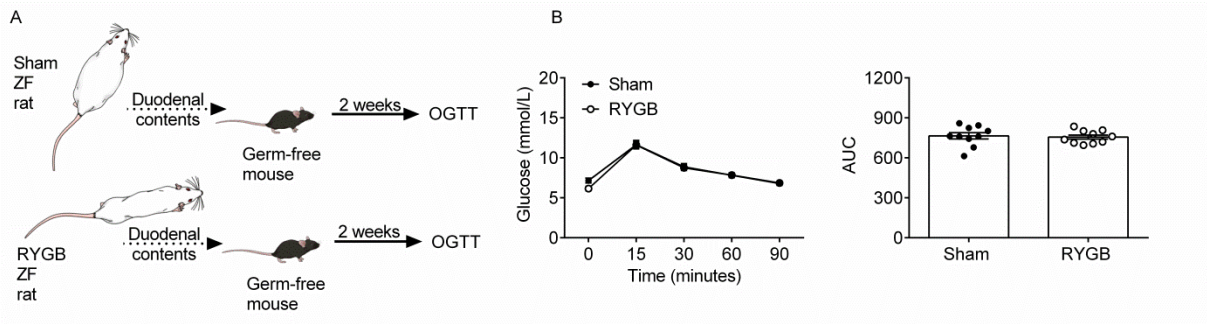

Figure S2. The Duodenal Contents of RYGB-Operated Rats Do Not Affect Glycemic Control in Recipient Germ-Free Mice, Related to Figure 2.

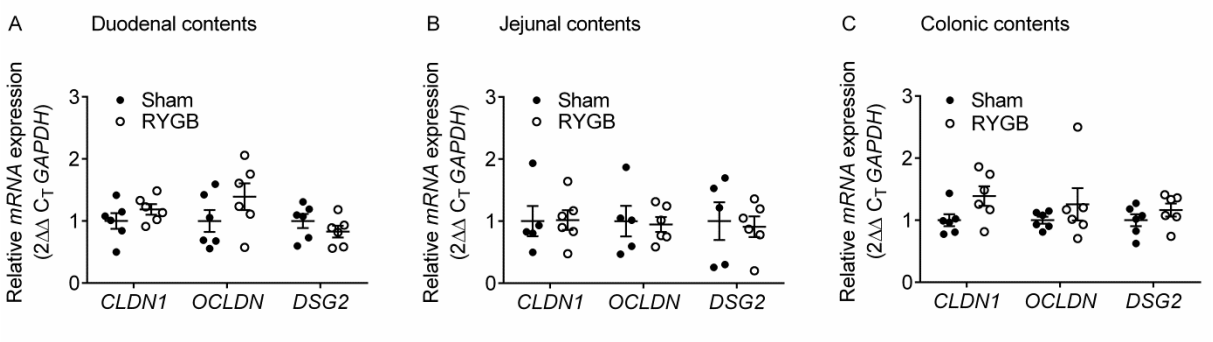

Figure S3. The Duodenal, Jejunal, and Colonic Contents of RYGB-Operated Rats Do Not Affect the Transcription of Barrier Proteins in Caco-2 Cells, Related to Figure 3.

Antibody	Source	Catalogue Number	Dilution (WB)	Dilution (IF)
Claudin-1	ThermoFisher Scientific, Waltham, USA	51-9000	1:250	1:50
Occludin	ThermoFisher Scientific, Waltham, USA	33-1500	1:500	1:50
Desmoglein-2	ThermoFisher Scientific, Waltham, USA	32-6100	1:250	1:50
β-actin-Peroxidase	Sigma-Aldrich, Munich, Germany	A3852	1:10000	1: 10000

Table S1. Primary Antibodies, Related to Figure 3.

Antibody	Source	Catalogue Number	Dilution (WB)	Dilution (IF)
Horseradish peroxidase labelled goat anti-mouse IgG	Dionova, Hamburg, Germany	115-035-003	1:3000	-
Horseradish peroxidase labelled goat anti-rabbit IgG	Dionova, Hamburg, Germany	111-035-003	1:3000	-
Dam Alexa Fluor 488	ThermoFisher Scientific, Waltham, USA	A-21201	-	1:200
Darb Alexa Fluor 488	ThermoFisher Scientific, Waltham, USA	A-21206	-	1:200

Table S2. Secondary Antibodies, Related to Figure 3.

Gene	Sequence
CLDN1	Forward: CCCAGTCAATGCCAGGTACG Reverse: CAAAGTAGGGCACCTCCCAG
OCLDN	Forward: CCCCATCTGACTATGTGGAAAG Reverse: CAGGCGAAGTTAATGGAAGC
DSG2	Forward: TTGAGGTCAATGAAGGGGTC Reverse: GAAGGTGAAGGTCGGAGTCA
GAPDH	Forward: TGCTGCTTCTCCTGATCTGCT Reverse: GATCCTCTCCCTCCCGAAGA

Table S3. Primer Sequences, Related to Figure 3.

TRANSPARENT METHODS

Animals

Thirty male Wistar rats (Charles River) aged 4 weeks and weighing 324.3 ± 2.8 g were initially group-housed in a dedicated facility with an ambient room temperature of 22^{o}C and a 12-hour light/dark cycle with lights on at 7 am. They were immediately placed on a high-fat diet (C1090-60, Altromin; 5. 2 kcal/g, 60 % kcal from fat, 16 % kcal from protein, and 24 % kcal from carbohydrate) for 5 weeks to induce obesity (body weight of 477.9 ± 6.9g) and were then randomly allocated to RYGB (n = 20; body weight of 474.2 ± 6.7 g) or sham operation (n = 10; body weight of 470.6 ± 10.1 g) groups as previously described (Seyfried et al., 2013). Briefly, anesthesia was induced with 5% isoflurane in 2% oxygen mix and maintained with 2% isoflurane in 2% oxygen mix. Animals then received 3mg/kg carprofen analgesia subcutaneously and 1.25mg/kg amoxicillin antibiotic intraperitoneally. For the RYGB procedure, a midline laporatomy was made and a small gastric pouch 5% of the original stomach size was anastomosed to the lower part of the transected mid-jejunum (15 cm away from the pylorus) in an end-to-side fashion to create the alimentary limb. The freed upper jejunum was anastomosed in a side-to-side fashion to the lower jejunum (25 cm away from the ileo-cecal valve) to create the biliopancreatic limb (Figure S1). For the sham procedure, a midline laparotomy was made and a 1 cm longitudinal gastrostomy was performed along the anterior wall of the stomach with subsequent closure.

Following surgeries, rats were transferred to individual cages and for the first 3 post-operative recovery days were only given a liquid diet (Vanilla-flavored Ensure; 0.93 kcal/mL 22 % kcal from fat) and 3mg/kg carprofen analgesia subcutaneously. From post-operative day 4 onwards, rats were given simultaneous free access to both low-fat (Altromin, C1090-10; 3. 5 kcal/g, 10 % kcal from fat, 24 % kcal from protein, and 66 % kcal from carbohydrate) and high-fat diets to model the real-world situation in humans and assess changes in food choice (Dischinger et al., 2019; Hankir et al., 2017). High-fat and low-fat diet intakes were then measured daily for the subsequent 17 days and high-fat diet preference was calculated by dividing the amount of kcal of high-fat diet consumed with the total kcal consumed and expressed as percentage. Five RYGB-operated rats exceeded tolerable weight loss limits within 7 days of surgeries and were therefore humanely sacrificed. Post-mortem revealed leakage of their lower (side-to-side) anastomoses.

At the 6th post-operative week, plasma was separated from trunk blood from a subset of 12-hour fasted rats (n = 6 sham-operated and n = 5 RYGB-operated) by centrifugation at 5 krpm for 10 minutes in tubes containing EDTA and stored at -80°C. The gastrointestinal tract was dissected from these same rats and cut into 10 cm duodenal, mid-jejunal, and colonic segments for sham-operated rats, and equivalent regions (biliopancreatic limb, alimentary limb, and colon) for RYGB-operated rats (Figure S1). The contents from each intestinal segment were collected in cryotubes which were immediately snap-frozen in liquid nitrogen and stored at -80°C. All procedures were approved by the local regulatory authority (Regierung von Unterfranken: 55.2-2532-2-467).

Intestinal contents transfer experiments

Sixteen germ-free C57/bl6 male mice aged 10 weeks and maintained on an autoclaved, standard chow diet were used for the jejunal and colonic contents transfer experiments as previously described (Arora et al., 2017). Briefly, the frozen jejunal and colonic contents of RYGB-operated and sham-operated rats were pooled and homogenized in phosphate-buffered saline (PBS) supplemented with reducing solution (1% cysteine dissolved in $NaHCO_3$ buffer). The resultant slurry (200 µL) was orally gavaged into 4-hour fasted germ-free mice (n = 4-5/group for the jejunal contents and n = 3-4/group for the colonic contents) who were subsequently maintained in autoclaved individual ventilated cages with sterile bedding and fed autoclaved food and water *ad libitum* for the next 2 weeks. On day 14, an OGTT was performed on 4-hour fasted mice by oral administration of 30 % d-glucose (2 g/kg body weight). Blood was drawn from the tail vein at 0, 15, 30, 60, and 90 minutes, and blood glucose levels were measured with a Bayer glucometer. One measurement at t = 30 minutes for a mouse that received the colonic contents from sham-operated rats was excluded as it was > 30 % lower than the others in the group (9.25 mmol/L vs 14.30 mmol/L and 14.90 mmol/L). Immediately following the OGTT, serum was isolated from trunk blood by centrifugation at 5 krpm for 10 minutes and stored at -80°C. Duodenal contents transfer experiments from genetically obese and glucose-intolerant ZF rats were performed as previously described (Arora et al., 2017). All procedures were approved by the Danish Animal Research authorities issued by the Danish Committee for Animal Research.

Patient plasma samples

Twelve-hour fasting plasma samples were previously obtained from a longitudinal patient cohort (Bankoglu et al., 2018). Patients (30 females, 8 males) were 43.8 ± 1.6 years of age at

the time of RYGB, of whom 12 were diagnosed with type 2 diabetes according to American Association of Diabetes criteria (Bankoglu et al., 2018). Plasma samples were obtained from these patients immediately prior to a standard 2-4 week very low calorie diet (1, 000 kcal per day) which comprised 2 daily liquid meals (such as egg white shakes or vegetable soup) and 1 daily solid meal (such as tuna fish or chicken breast salads) that were low in fat and carbohydrates and rich in protein (100g) and also at 12 months follow-up. Sample sizes for each measured parameter at each time-point can be found in Tables 1 and 2. The original study was approved by the Ethics Committee of the University of Wuerzburg (Study No: 186/14).

Immunoassays

For animal samples, plasma insulin was measured using an Ultrasensitive Rat Insulin ELISA Kit (10-1251-01, Mercodia; 1:100 dilution), plasma LPS using a Limulus Amebocyte Lysate Chromogenic Endpoint Assay (HIT302, HycultBiotech; 1:10 dilution), and serum LBP using a Mouse LBP ELISA Kit (HK205-01, HycultBiotech; 1:500 dilution). For human samples, plasma insulin, leptin, TNF-α, and Il-6 were measured using a MILLIPLEX MAP Human Adipokine Magnetic Bead Panel 2 – Endocrine Multiplex Assay (HADK2MAG-61K-05, Merck; undiluted), plasma LPS using the same Limulus Amebocyte Lysate Chromogenic Endpoint Assay (HIT302, HycultBiotech; 1:10 dilution) as for the rat samples, and plasma FGF19 using a Human FGF19 ELISA Kit (ab230943, Abcam; 1:2 dilution).

Bile acid measurements

Bile acids (cholic acid, chenodeoxycholic acid, alpha/beta-muricholic acid, omega-murichoclic acid, lithocholic acid, hyodeoxycholic acid, ursodeoxycholic acid, glycocholic acid, glycochenodeoxycholic acid, taurocholic acid, taurochenodeoxycholic acid, tauromuricholic acid (sum of alpha and beta), glycodeoxycholic acid, glycolithocholic acid, taurodeoxycholic acid, taurolithocholic acid, glycoursodeoxycholic acid and tauroursodeoxycholic acid) were quantified using a Bile Acids Kit® (BIOCRATES Life Sciences). Electrospray ionization liquid chromatography–mass spectrometry (ESI-LC-MS/MS) was performed on a Sciex 4500QTRAP MD MS-system coupled to an Agilent 1290 UHPLC-system (G4226A autosampler, infinity binpump, G1316C column-oven, G1330B thermostat) according to the manufacturer's recommendations (UM-BA-SCIEX-16). MS data was validated and processed with MetIDQ™ (7.13.11-DB109-Nitrogen-2850) and Analyst® (1.6.2 MD) software. Alpha/beta-muricholic, hyodeoxycholic, and taurine-conjugated bile

acids were excluded from further analysis as they were below threshold levels of detection for most samples.

Drugs

WAY-362450 (1749, Axon Medchem), DY-268 (2561, Axon Medchem), Triamterene (T4143, Sigma), and 3-(2-chlorophenyl)-N-(4-chlorophenyl)-N,5-dimethyl-4-isoxazolecarboxamide (16291, Cayman Chemicals) were dissolved in 100% DMSO as 10 mM stock solutions and stored in aliquots at -20^{o}C.

Intestinal contents preparation for cell culture experiments

Frozen duodenal (mainly fluid) contents were dissolved in distilled water at a concentration of 100mg/mL, whereas frozen jejunal and colonic (mainly solid) contents were dissolved in distilled water at a concentration of 100mg/1.5mL. After vigorous mixing in a TissueLyzer (Qiagen) for 10 minutes, the resultant slurries were centrifuged at 13 krpm for 10 minutes at 4^{o}C. Supernatants were filtered through a 70 µm nylon cell strainer (Falcon), pooled for RYGB-operated and sham-operated groups, and stored in aliquots at -20^{0}C.

Cell culture

All cell culture was performed at 37^{0}C in a 5 % CO_2 and 95 % O_2 atmosphere. Commercially available (HTB-37, American Type Cell Culture) colorectal adenocarcinoma (Caco-2) cells originally derived from a 72 year-old male were grown to confluent monolayers in Dulbecco's Modified Eagle's Medium (DMEM) (D5796, Sigma) supplemented with 50 U/mL penicillin-G, 50 µg/mL streptomycin, and 10 % fetal calf serum (FCS) (Biochrom). For all experiments, FCS was substituted for 10 % intestinal contents.

Measurement of TER

Caco-2 cells were seeded onto 8-well chambers (72040, 8W10E+ PET, Applied Biophysics) and grown to confluent monolayers. DMEM supplemented with the intestinal contents was then applied and low-frequency measurements (400 Hz, 600s interval), reflecting resistance between cells (Robilliard et al., 2018), were immediately made for 24 hours using the Electric Cell Impedance Sensor (ECIS) Trans-Filter Adapter 1600R System (Applied Biophysics). Data are expressed as percentage relative to baseline for each treatment condition.

Measurement of 4 kDa FITC–dextran flux.

Caco-2 cells were seeded onto trans-well chambers (353180, 0.4 μm pore size; Falcon) in 6-well plates and grown to confluent monolayers. DMEM supplemented with the intestinal contents was then applied for 24 hours followed by incubation for 2 hours with fresh clear DMEM (D1145, Sigma) containing 10 mg/mL 4 kDa FITC-dextran (Sigma). Paracellular flux of 4kDa FITC-dextran was assessed by taking 50 μL aliquots from the outer chamber at baseline and 100 μL aliquots from the inner chamber at 60 minutes. Fluorescence was measured using a spectrophotometer with excitation and emission wavelengths of 485 nm and 535 nm, respectively. Permeability coefficients (P_E) were calculated as previously described (Brun et al., 2015).

Immunoblotting

Caco-2 cells were seeded onto 6-well plates and grown to confluent monolayers. DMEM supplemented with the intestinal contents was then applied for 24 hours and Caco-2 cells were homogenized in SDS lysis buffer containing 25 mM HEPES, 2 mM EDTA, 25 mM NaF, 1 % SDS and 1 % protease inhibitor cocktail (ThermoFisher). SDS gel electrophoresis and blotting were performed after normalization of protein amount using the bicinchoninic acid (BCA) assay (ThermoFisher), as previously described (Meir et al., 2019). Primary and secondary antibodies were diluted as detailed in Tables S1 and S2 in 5 % milk and 0.1 % Tween. Bound immunoglobulins were visualized by enhanced chemiluminescence (Amersham) and quantified by densitometry (ChemicDoc Touch Bio-Rad Laboratories), normalized to a reference protein (β-actin), and expressed relative to the Sham group.

Immunofluorescence

Caco-2 cells were seeded onto glass coverslips and grown to confluent monolayers. DMEM supplemented with the intestinal contents was then applied for 24 hours and Caco-2 cells were prepared for immunostaining as previously described (Meir et al., 2019). Primary and secondary antibodies were diluted as detailed in Tables S1 and S2. Images with a field of view (FOV) of 135μm x 135μm were generated using a Zeiss LSM 780 confocal microscope at 60 x magnification. For each treatment condition, image analysis was performed on 4 random FOVs with Image J software (https://imagej.nih.gov/ij/index.html). For each FOV, signal intensity was measured along 8μm lines drawn orthogonally across cell borders and averaged. Background signal intensity was similarly measured in the intracellular space in

each FOV, averaged, and subtracted from the average signal intensity across cell borders. The resulting curves were then integrated to obtain mean signal intensities for each FOV.

RT-qPCR

Caco-2 cells were seeded onto 6-well plates and grown to confluent monolayers. DMEM supplemented with the intestinal contents was then applied for 24 hours and Caco-2 cells were homogenized in Rneasy^{TM} Lysis Buffer (Qiagen). Total RNA was extracted using an Rneasy^{TM} plus micro-kit with on-column Dnase treatment to remove residual genomic DNA (Qiagen). RNA concentration was determined using a Nanodrop^{TM} 2000C spectrophotometer (ThermoFisher) and 1µg was reverse transcribed using an iScript^{TM} cDNA synthesis kit (Biorad) on a primus 96 thermocycler (Peqlab) set at 55^{o}C for 40 minutes. 100ng cDNA was loaded in duplicate for each qPCR reaction using a MESA GREEN MasterMix Plus for SYBR^{TM} Assay kit (Eurogentec) and 100pmol forward and reverse primers (Eurofins) on a CFX96 touch real-time detection system (Biorad) with an annealing temperature of 60^{0}C and an elongation temperature of 72^{o}C (40 cycles). The ΔΔ Ct method was used to quantify mRNA expression of the gene of interest normalized to a reference gene (glycerinaldehyde-3-phosphate-dehydrogenase-*GAPDH*) and expressed relative to the Sham group. Primer sequences are shown in Table S3.

Statistics

Data are presented as mean ± S.E.M. unless otherwise stated. All statistical tests were performed on GraphPad Prism 8.0 software. Two-tailed, unpaired *t*-test was applied to data with equal variance as determined by F-test and with Welch's correction to data with unequal variance. One-way ANOVA with Tukey's post-hoc test was applied to data when more than one comparison was made. Two-way ANOVA with Sidak's post-hoc test was applied to data with two independent variables. Two-tailed, paired *t*-test was applied to normally distributed longitudinal data as determined by D'Agostino & Pearson test and Wilcoxan matched-pairs signed rank test was applied to non-normally distributed longitudinal data. A P value of $\leq$ 0.05 was considered statistically significant.

SUPPLEMENTARY REFERENCES

Arora, T., Seyfried, F., Docherty, N.G., Tremaroli, V., le Roux, C.W., Perkins, R., and Backhed, F. (2017). Diabetes-associated microbiota in fa/fa rats is modified by Roux-en-Y gastric bypass. ISME J. 11, 2035-2046.

Brun, P., Gobbo, S., Caputi, V., Spagnol, L., Schirato, G., Pasqualin, M., Levorato, E., Palu, G., Giron, M.C., and Castagliuolo, I. (2015). Toll like receptor-2 regulates production of glial-derived neurotrophic factors in murine intestinal smooth muscle cells. Mol. Cell. Neurosci. 68, 24-35.

Dischinger, U., Corteville, C., Otto, C., Fassnacht, M., Seyfried, F., and Hankir, M.K. (2019). GLP-1 and PYY3-36 reduce high-fat food preference additively after Roux-en-Y gastric bypass in diet-induced obese rats. Surg. Obes. Relat. Dis. 15, 1483-1492.

Hankir, M.K., Seyfried, F., Hintschich, C.A., Diep, T.A., Kleberg, K., Kranz, M., Deuther-Conrad, W., Tellez, L.A., Rullmann, M., Patt, M., et al. (2017). Gastric Bypass Surgery Recruits a Gut PPAR-alpha-Striatal D1R Pathway to Reduce Fat Appetite in Obese Rats. Cell Metab. 25, 335-344.

Meir, M., Burkard, N., Ungewiss, H., Diefenbacher, M., Flemming, S., Kannapin, F., Germer, C.T., Schweinlin, M., Metzger, M., Waschke, J., et al. (2019). Neurotrophic factor GDNF regulates intestinal barrier function in inflammatory bowel disease. J. Clin. Invest. 129, 2824-2840.

Robilliard, L.D., Kho, D.T., Johnson, R.H., Anchan, A., O'Carroll, S.J., and Graham, E.S. (2018). The Importance of Multifrequency Impedance Sensing of Endothelial Barrier Formation Using ECIS Technology for the Generation of a Strong and Durable Paracellular Barrier. Biosensors 8, 64.

Seyfried, F., Miras, A.D., Bueter, M., Prechtl, C.G., Spector, A.C., and le Roux, C.W. (2013). Effects of preoperative exposure to a high-fat versus a low-fat diet on ingestive behavior after gastric bypass surgery in rats. Surg. Endosc. 27, 4192-4201.